survivability was assessed by MTT [3-(4,5-dimethylthiazol-2-yl)-2,5-diphenyl tetrazolium bromide] assay [39] per the manufacturer's instructions (TACS™, R&D systems, MN, USA). In the UV-treated cells, 10 μl of MTT solution was added to each well, and the plates were incubated at 37 °C for 4 h. Subsequently, 100 μl of detergent reagents were added to each well to dissolve the formed blue formazan. In the US-treated cells, 25 μl of MTT solution was added to each well, and the plates were incubated at 37 °C for 4 h, followed by the addition of 250 ml of detergent reagents. After the formazan was completely dissolved, the formazan solution was transferred to a 96-well plate. The absorbance of 570 nm for the formazan solution was measured using the SUNRISE™ microplate reader (TECAN, Kawasaki, Japan). Treated and non-treated control wells were compared. The survival rate of the cells was calculated by the following formula:

$$\%\text{Survival rate} = [\text{absorbance of treated group}/\text{absorbance of control group without any treatment}] \times 100$$

### 2.6. Inhibition of cytotoxic oxidative radical

The effect of an oxidative radical scavenger on both UV and US irradiation in the presence of $TiO_2$/PEG was tested. Glutathione (SIGMA®, MO, USA) was used as a radical scavenger. After 3 h incubation of the cells in medium containing 100 μg/ml of $TiO_2$/PEG with various concentrations of glutathione (10–20 mM), the cells were irradiated by UV (5.0 mW/cm$^2$, 60 min) or US ($I_{SATA}$; 1.0 W/cm$^2$, 50 s). The treated cells were stored at 37 °C for 24 h. The cell survivability was assessed by MTT assay.

### 2.7. Immunofluorescence staining

To assess the viability and damage of U251 cells after UV irradiation for 60 min or US irradiation ($I_{SATA}$; 1.0 W/cm$^2$) for 50 s with 100 μg/ml $TiO_2$/PEG diluted in DMEM, the irradiated cells were stained with Calcein AM/ Ethidium homodimer co-staining kit (Live/Dead Viability/Cytotoxicity assay kit®, Invitrogen, OR, USA). The cell-permeate esterase substrate Calcein AM is non-fluorescent until enzymatically converted to highly fluorescent Calcein (excitation 494 nm, emission 517 nm), which is retained within live cells. Ethidium homodimer-1 (EthD-1, excitation 528 nm, emission 617 nm) undergoes fluorescence enhancement upon binding nucleic acids. This dye is excluded from cells that have an intact plasma membrane. On the other hand, they can penetrate the membranes of dead cells and intercalate into nuclear deoxyribonucleic acid (DNA). For double staining with Calcein AM and EthD-1, after washing the cells with PBS solution on a 24-well plate, PBS containing 2 μM of Calcein AM and 4 μM of EthD-1 was added to each well, and cells were incubated for 30 min at room temperature in the dark. Cells were washed twice by PBS and observed using fluorescent microscopy (IX71, U-LH100HGPO, Olympus, Tokyo, Japan).

To assess the cell damage mechanism by UV and US irradiation, the treated cells were stained with Annexin V-FITC and Propidium iodide (PI) (Annexin V-FITC Apoptosis Kit, BioVision, CA, USA). The acute phase of apoptosis is accompanied by translocation of phospholipids, which are normally restricted to the inner surface of the cell membrane, to the outer leaflet of the still intact cell membrane, where they can be recognized by Annexin V (excitation 490 nm, emission 518 nm). The nucleus is stained with PI (excitation 536 nm, emission 620 nm), which penetrates the damaged cell membrane. U251 cells, which were treated with UV for 60 min or US for 50 s with 100 μg/ml $TiO_2$/PEG or without $TiO_2$/PEG in a 24-well plate, were washed twice with PBS, followed by 500 μl of cold binding buffer containing 5 μl Annexin V-FITC and 5 μl PI, and were incubated for 15 min at room temperature in the dark. Cells were washed twice and then evaluated with fluorescent microscopy. This double staining procedure (Annexin V-FITC and PI) was performed 6 h after irradiation in order to assess the pattern of cell damage. For quantification of the staining pattern, the percentages of stained cells (Annexin V-FITC only, PI only, and both) were determined in high power field images (×400) created by digitally merging fluorescence images and phase-contrast images.

Further, the US-treated and UV-treated cell membranes were labeled by Vybrant® Dil (excitation 549 nm, emission 565 nm, Lonza, MD, USA) for assessment of the sonotoxic damage of the cell membrane. Vybrant® Dil has the highly lipophilic nature of carbocyanine dyes and stains viable cell membranes. Cell nuclei were labeled with Hoechst 33342 (excitation 350 nm, emission 461 nm, Invitrogen), which can bind DNA regardless of cell survival. Immediately after US or UV irradiation, treated U251 cells were washed twice with PBS, and then the cells were incubated in DMEM containing 50 μM Vybrant® Dil at 37 °C for 10 min. After rinsing with PBS, the cell nuclei were labeled by Hoechst 33342 (0.1 mg/ml final concentration in PBS) at room temperature for 10 min and observed with fluorescent microscopy.

### 2.8. Statistical analysis

Data in figures is expressed as mean ± standard deviation. Statistical analysis was performed with Statcel2 software (OMS publishing Inc, Saitama, Japan). Differences between the groups were considered significant when P-values of one-way analysis of variance (ANOVA) followed by Bonferroni test for the post hoc determination of significant differences were less than 0.01.

## 3. Results

### 3.1. Sonodynamic anti-tumor effect

The cytotoxicity of $TiO_2$/PEG induced by various intensities of US ($I_{SATA}$; 0.4–1.2 W/cm$^2$, 30 s) was tested on U251 cells by MTT assay (Fig. 1). Minor cytotoxicity at high US intensity was observed

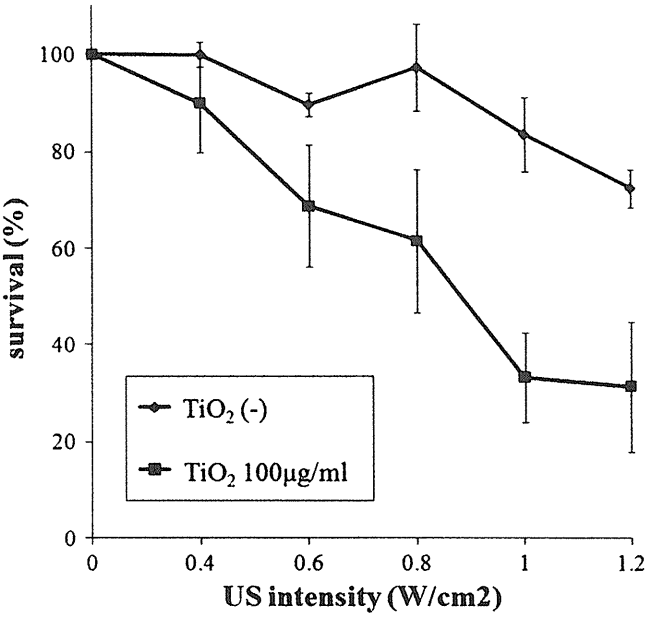


**Fig. 1.** The surviving fraction of U251 cells as a function of US intensity with or without $TiO_2$/PEG diluted in DMEM. Cell survival rate was measured by MTT assay 24 h after US irradiation. US frequency was 1 MHz with 50% duty ratio, and irradiation time was 30 s. Bars in the figure represent average ± standard deviations.

even without $TiO_2$/PEG in the medium. In the presence of 100 μg/ml $TiO_2$/PEG, the cell survival rate remarkably decreased depending on US intensity. $TiO_2$/PEG itself (without US exposure) showed no cytotoxic effect on U251 tumor cells (data not shown).

### 3.2. Comparison between sonodynamic and photodynamic effect of $TiO_2$/PEG on cell survival

Fig. 2 shows the influences of irradiation time on survival rate of the treated U251 cells. Throughout this comparison, the intensity ($I_{SATA}$) of US irradiation was fixed at 1.0 W/cm$^2$ because our first experiment showed that the difference of survival rates in the absence and presence of $TiO_2$/PEG was largest at this setting (Fig. 1). Cytotoxicity was not confirmed in the group that underwent UV irradiation alone (Fig. 2a). In the US irradiation group, a slight suppression was seen in the group that underwent US exposure even without $TiO_2$/PEG, and the sonocatalytic cytotoxic effect remarkably increased with $TiO_2$/PEG. In the presence of $TiO_2$/PEG, the photodynamic cytotoxic effect was not observed until the UV light dose exceeded 6.0 J/cm$^2$ (UV irradiation time; 20 min), while the sonodynamic cytotoxicity effect was almost proportional to the duration of US irradiation. The surviving fraction was reduced to about 10% after 60 min of UV irradiation time and 50 s of US irradiation time, respectively.

### 3.3. The inhibiting effects of oxidative radical scavenger

To investigate the influences of oxidative radicals for cytotoxicity induced by UV irradiation and US irradiation in the presence of 100 μg/ml $TiO_2$/PEG, the effect of 10–20 mM of glutathione, an active oxidative radical scavenger, on cell survival was tested. Fig. 3 demonstrates cell survival rate at 60 min after UV irradiation and at 50 s after US irradiation ($I_{SATA}$; 1.0 W/cm$^2$). In the UV irradiation group, the cell damages were obviously inhibited by glutathione (Fig. 3a, $^{\#\#}p < 0.01$)). In the US irradiation group, glutathione did not inhibit cell killing in comparison to the control (Fig. 3b, $^{**}p < 0.01$). On the other hand, glutathione relatively inhibited cell killing at 20 mM compared to 0 mM (Fig. 3b, $^{\#\#}p < 0.01$). These findings suggested that the influence of reactive oxidative radicals in the cell damage mechanism of SDT might be different from PDT.

### 3.4. The differences of mechanism in anti-tumor activities between sonodynamic treatment (SDT) and photodynamic treatment (PDT)

To investigate the mechanism of U251 cell damage by PDT and SDT with $TiO_2$/PEG, UV- or US-treated cells were stained with Calcein (green) and EthD-1 (red) to distinguish between viable cells and dead cells in the presence of 100 μg/ml $TiO_2$/PEG (Fig.4). Immediately after treatment, minimal cytotoxicity was observed in UV-treated cells, while approximately more than half of US-treated cells were stained with EthD-1. Twenty-four hours after treatment, almost all treated cells in both groups were negative for Calcein.

In addition, the cell death mechanism was tested by double staining with Annexin V-FITC and PI using fluorescent microscopy 6 h after irradiation (Fig. 5 and 6). In the absence of $TiO_2$/PEG, several US-treated cells were positive for PI (less than 20%) although there were scarcely any fluorescence signals from the UV-treated cells. In the presence of $TiO_2$/PEG, the cell membranes were clearly stained with Annexin V-FITC and the nucleus was also stained with PI, implying apoptotic changes of these cells in both UV-treated and US-treated cells. More than 50% of UV-treated cells were stained with both PI and Annexin V-FITC, indicating that the pathway of cell death was predominantly apoptosis. On the other hand, approximately 40% of US-treated cells were stained only with PI, suggesting that death is not only the result of apoptosis (Fig. 6).

Furthermore, the damage of cell membrane by US exposure in the presence and absence of $TiO_2$/PEG was analyzed by Vybrant® Dil staining (Fig. 7). Immediately after UV irradiation, the cell membrane with cellular processes was labeled by Vybrant® Dil regardless of whether $TiO_2$/PEG was present or absent (Fig. 7, upper). In the ultrasound alone group (without $TiO_2$/PEG), the cell membrane also maintained viability. On the other hand, the fluorescence signals decreased or disappeared immediately after US exposure in the presence of $TiO_2$/PEG (Fig. 7, lower). This result also demonstrated that the damage of cell membrane by $TiO_2$/PEG mediated SDT was completed quickly.

## 4. Discussion

First, results achieved in this study strongly suggested that $TiO_2$/PEG could be a novel sensitizer for SDT, because cell damage

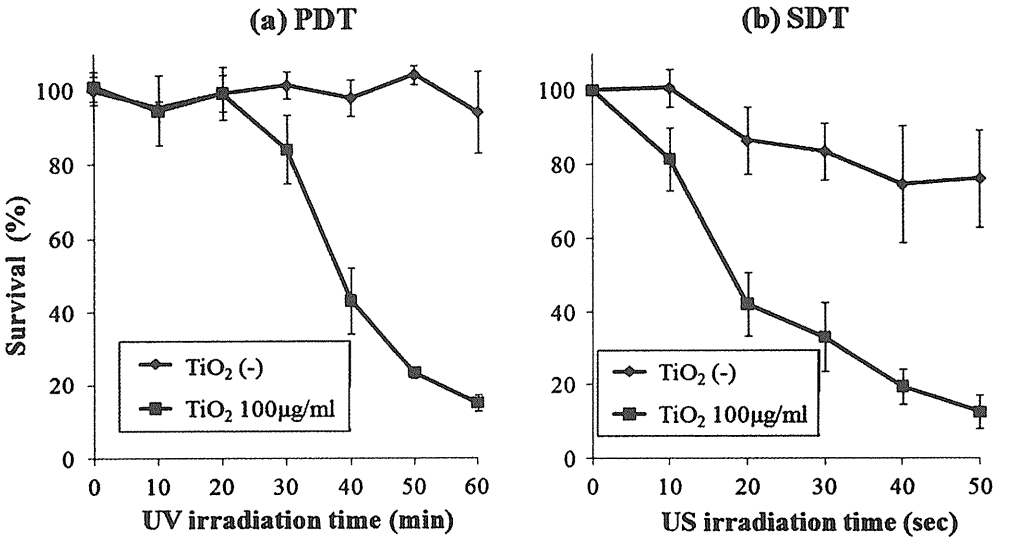


**Fig. 2.** The surviving fraction of U251 cells as a function of UV (a) and US (b) irradiation time. The cells were treated with or without $TiO_2$/PEG. The concentration of $TiO_2$/PEG was 100 μg/ml. UV light intensity was 5.0 mW/cm$^2$, and US intensity was 1.0 W/cm$^2$ in reading output.

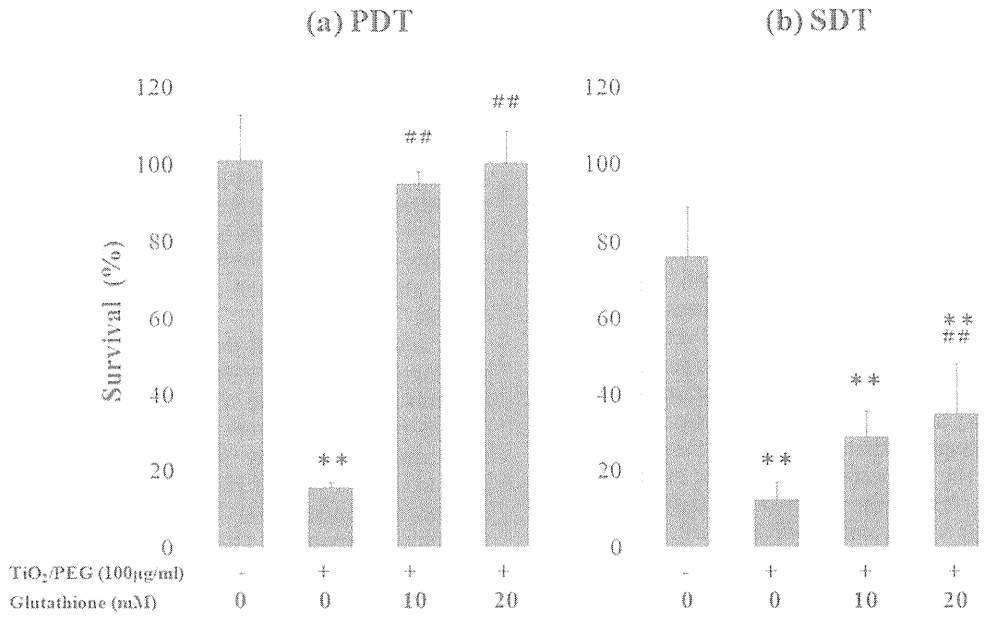


Fig. 3. The effect of a radical scavenger (glutathione) on cytotoxicity 60 min after UV irradiation (a) and 50 min after US irradiation (b). The concentration of $TiO_2$/PEG was 100 μg/ml. The data are expressed as the mean ± standard deviation ($n$ = 10–12), and statistical analysis was performed using one-way ANOVA followed by Bonferroni test. ** shows a significant difference ($p < 0.01$) between the control ($TiO_2$(−) and glutathione(−)) and each treatment. ## shows a significant difference ($p < 0.01$) between the non glutathione ($TiO_2$(+) and glutathione(−)) group and the glutathione-treatment group ($TiO_2$(+) and glutathione(+)). Cell damage in PDT was completely inhibited by both concentrations of glutathione (a), while the scavenger did not reduce cell death induced by SDT (b).

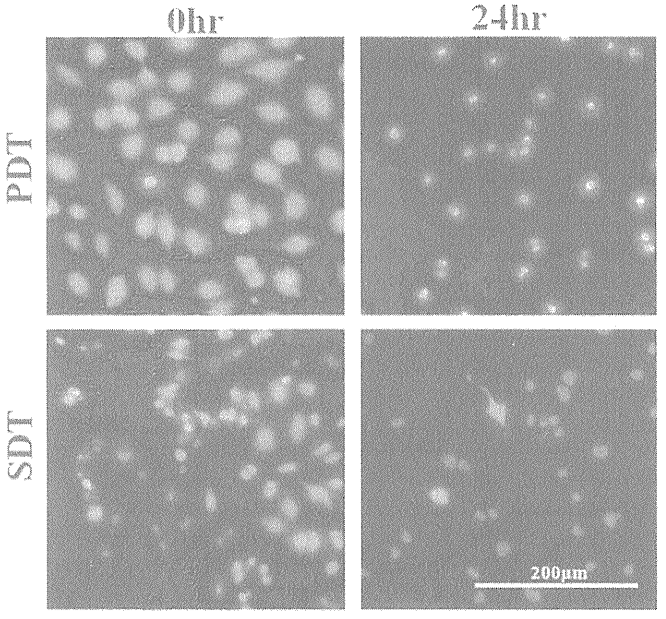


Fig. 4. Double immunostaining for Calcein (green) and Ethidium homodimer-1 (red) of treated cells with $TiO_2$/PEG for 60 min UV irradiation (upper) and 50 s US irradiation (lower). The concentration of $TiO_2$/PEG was 100 μg/ml. Immediately after treatment, UV-treated cells were stained with Calcein, while many US-treated cells were already stained with Ethidium homodimer-1 (left). Twenty-four hours after treatment, almost all treated cells were not stained with Calcein in both PDT and SDT groups (right).

induced by ultrasonic treatment was remarkably enhanced by $TiO_2$/PEG in vitro.

Furthermore, we attempted to compare $TiO_2$/PEG mediated SDT and PDT. The output irradiation intensity was set at 1.0 W/cm$^2$ (reading output power), for 50 s because the approximately 90% cell killing effect (measured by MTT assay) at this level of US energy corresponded to the UV exposure experiment (approximately 90% cell killing effect with 5.0 mW/cm$^2$ for 60 min). However, with US irradiation, the buffer (6% acrylamide gel) was inserted between the US transducer and the well plate to avoid an increase in temperature of the culture medium. It is assumed that actual energy to the glioma cells on the well plate was reduced.

According to the measurement using the membrane hydrophone, insertion of the buffer gel and the base plate of the well decreased US intensities applied to glioma cells to 74.6%. Therefore, the US intensity of 1 W/cm$^2$ in reading output is estimated to be 0.59 W/cm$^2$ in $I_{SATA}$ in the condition with no standing wave generation. In the practical experimental condition, however, strong reflection at a water–air interface and well walls causes generation of a standing wave inside the well, resulting in enhanced effects of US exposure. Although it is difficult to predict intensity distributions in the plastic wells with standing wave, it is important to determine whether inertial cavitation was produced. Feril et al. investigated US-induced apoptosis with the same type of ultrasonic apparatus (SONIC MASTER ES-2, OG-Giken) and a similar US exposure configuration using a culture dish [40]. They evaluated US-induced free radicals (hydroxyl radical) by electron paramagnetic resonance (EPR) analysis and confirmed the presence of free radicals at intensities above 0.3 W/cm$^2$ with 10% duty ratio ($I_{SATA}$; 0.081 W/cm$^2$) and increases with increasing intensity. Based on their experiment, the effective US intensities applied to cells in our sonodynamic treatment condition should be above the threshold for inertial cavitation, accounting for the decline of US intensity by the buffer gel and the base plate of the well.

Since a direct comparison of PDT and SDT is difficult, this study demonstrated one aspect of various conditions. Nevertheless, this kind of comparison is still important and is the first step for clinical development of SDT in glioma therapy as many photosensitizers such as porphyrin derivatives have been converted into sonosensitizers [11–18].

The sonodynamic cytotoxicity on U251 cells was almost proportional to the duration of US exposure. In contrast, photodynamic cytotoxicity seemed to have a threshold UV energy dose. Kessel et al. compared the effects of photodynamic and sonodynamic cytotoxicity mediated by mesoporphyrin. They found differences

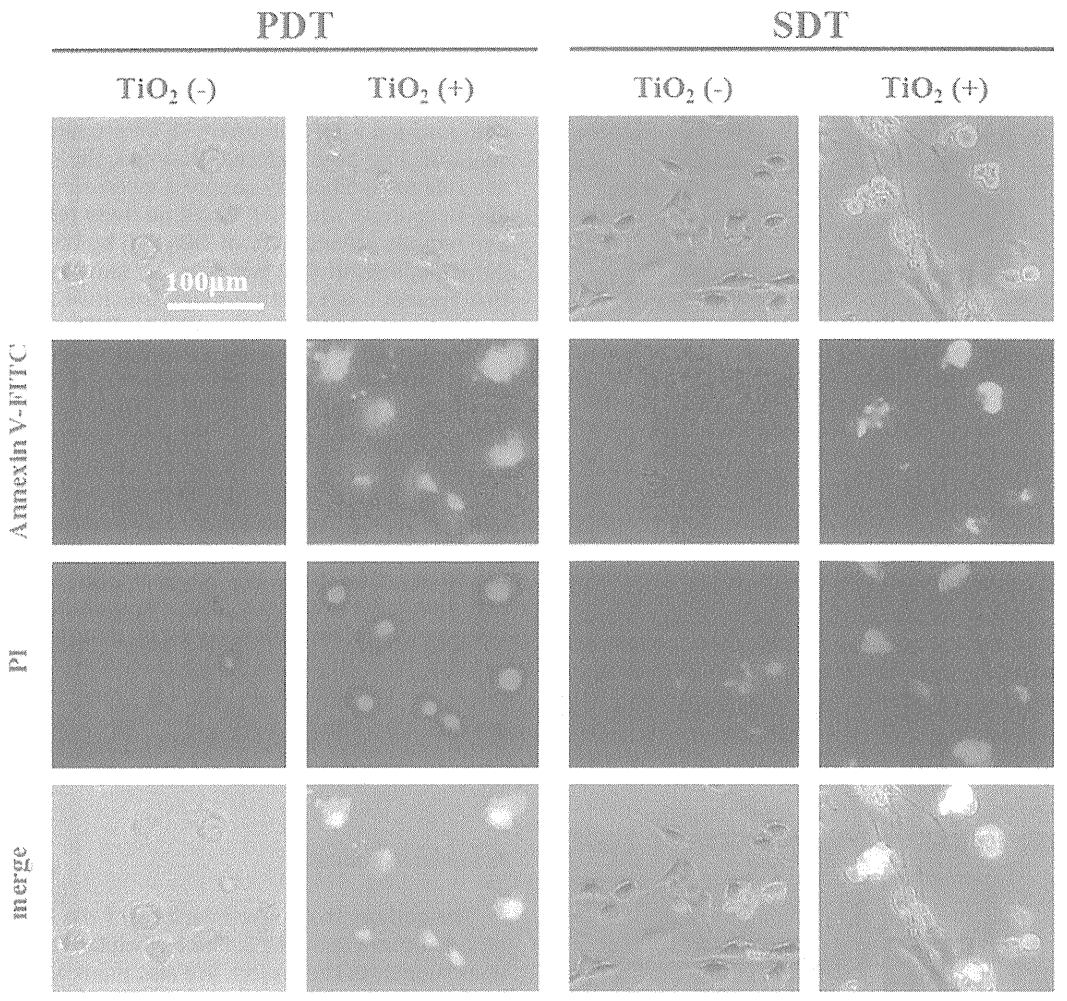


Fig. 5. The figures show the phase-contrast (upper), fluorescent (2nd and 3rd lines) and merged (lower) microscopic images of the PDT and SDT cells 6 h after irradiation. The cells were stained with Annexin V-FITC (green) and Propidium iodide (PI) (red). "$TiO_2(-)$" means irradiation in the absence of $TiO_2$/PEG, and "$TiO_2(+)$" means irradiation using the culture medium containing 100 μg/ml $TiO_2$/PEG. In the $TiO_2(-)$ group, several US-treated cells were stained with only PI. In both PDT and SDT with the $TiO_2$/PEG, the cell membranes were clearly stained with Annexin V-FITC, and the nuclei were also stained with PI.

in cytotoxic activity between photo and US treatments [36], and their result was basically identical to ours. They suspected that the threshold in the photodynamic cytotoxic effect may indicate the capacity for limited repair of photodamage, and US-induced loss of viability results from rapid cell destruction and is proportional to the time of US exposure. In distinguishing the mechanisms of PDT and SDT, formation of a singlet oxygen has been one of the most important issues. In the present study, glutathione, a singlet oxygen scavenger, almost completely inhibited photodynamic cytotoxicity of $TiO_2$/PEG. Reactive oxidizing radicals, such as hydroxyl radicals, superoxide anion and singlet oxygen are formed on photocatalytic $TiO_2$ in the aqueous environment [19,20,23,41]. These oxidative radicals are expected to be toxic to the tumor cells [42]. The inhibition of photodynamic cytotoxicity by glutathione indicated that oxidative radicals might play a primary role in cell damage in $TiO_2$/PEG mediated PDT.

On the other hand, with glutathione, the inhibition of sonodynamic cytotoxicity with $TiO_2$/PEG was limited. In recent years, the mechanism of sonodynamic therapy using sonosensitizers was not only due to an oxidizing chain reaction of cell membranes and cellular components by formation of oxidative radicals but also physical destabilization of the cell membrane by sonosensitizers. Thus, the cell was more susceptible to shear forces [35,43]. Our results suggested a series of oxidizing chain reactions by oxidative radicals was not a dominant cytotoxic mechanism of sonocatalytic therapy for glioma cells using $TiO_2$/PEG.

The fluorescence assays for cells treated by UV or US with $TiO_2$/PEG clearly indicated that the $TiO_2$/PEG mediated sonodynamic cytotoxic pattern is different from the photodynamic pattern. Staining with EthD-1 revealed that the majority of cells were damaged by $TiO_2$/PEG mediated SDT immediately after treatment, although in PDT groups, there were hardly any damaged cells. Further, $TiO_2$/PEG was expected to enhance rapid cell damage because only a fraction of cells treated by US alone (without $TiO_2$/PEG) were stained with EthD-1 (data not shown). Similarly, the fluorescence staining with Vybrant® DiI, which labels viable cell membrane, showed that US with $TiO_2$/PEG crucially damaged the cell membrane immediately after irradiation, whereas the viability of the cell membrane was preserved immediately after US irradiation without $TiO_2$/PEG. These results indicated that $TiO_2$/PEG mediated SDT can rapidly damage glioma cells by injury to the cell membranes. Generally, the most sensitive structures in the cell are biomembranes, and the mechanism of SDT-induced cell damage was mainly due to mechanical stress leading to physical disruption of the cell membrane by sensitizers such as porphyrin and rhodamine derivatives in the close vicinity of cells and cavitation bubbles [35]. It is also suspected that US irradiation with $TiO_2$ nanoparticles results in destruction of the secondary structure of protein molecules

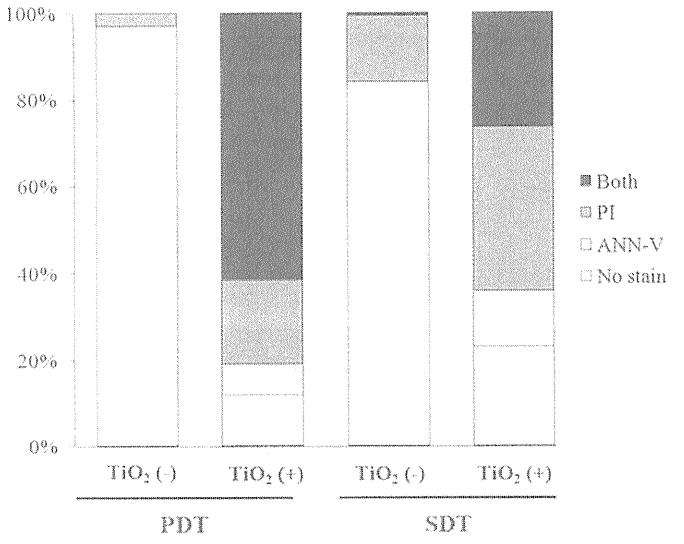


Fig. 6. The percentages of cells stained with Annexin V-FITC alone (ANN-V), Propidium iodide alone (PI) and both in each treatment 6 h after irradiation. The staining patterns of treated cells were determined by digitally-merged fluorescent and phase-contrast images. In the absence of $TiO_2$/PEG, UV-treated cells were hardly stained by Annexin V-FITC, and about 20% of US-treated cells were stained with only PI. In the presence of $TiO_2$/PEG, more than 50% of UV-treated cells were concomitantly stained with PI and Annexin V-FITC, while US-treated cells were predominantly stained with PI alone.

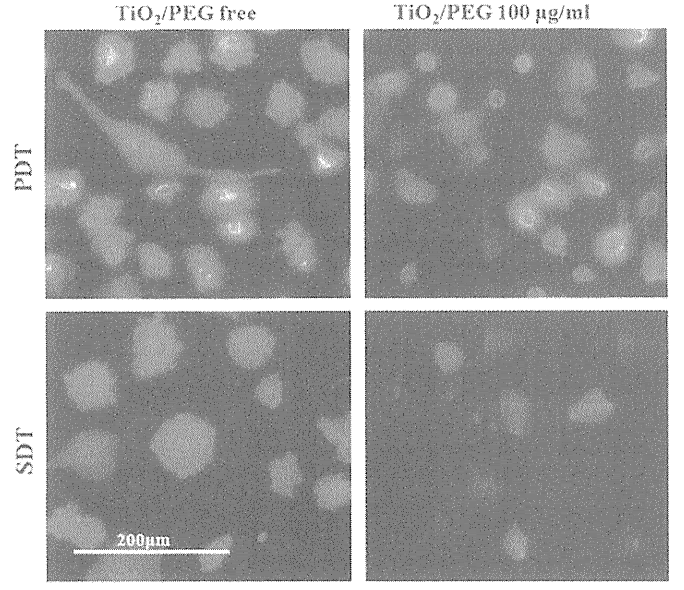


Fig. 7. The fluorescent micrographs demonstrate damage of the cell membrane immediately after UV irradiation (upper) and US irradiation (lower). The viable cell membranes were stained with Vybrant® DiI (red), and cell nuclei were stained with Hoechst 33342 (blue). The signals of Vybrant® DiI remarkably decreased after US exposure in the presence of $TiO_2$/PEG (lower right).

followed by loss of the space configuration, and the alteration of the configurations might cause forfeiture of their function [28]. In addition, the effect of SDT may depend on subcellular and intracellular localization of sonosensitizers. Hydrophilicity can be an important property of cell permeability of sensitizers [13], and $TiO_2$/PEG nanoparticles have colloidal stabilization and dispersibility in aqueous solution. Our previous investigations have shown that these nanoparticles might attach to tumor cell membranes and be incorporated in tumor cells [32]. This experimental result indicated that the water dispersed $TiO_2$/PEG exists in close vicinity of the cell membrane. This property results in physical disruption of cell membranes by sonocatalytic $TiO_2$/PEG and indicates that this nanoparticle might be suitable for sonodynamic therapy.

In both UV and US in the presence of $TiO_2$/PEG, cell staining with Annexin V-FITC occurred 6 h after treatment, suggesting that apoptosis had been induced. However, the radical scavenger was not able to significantly suppress cytotoxicity in SDT using $TiO_2$/PEG in contrast with PDT. Based on these results, although oxidative radicals generated from $TiO_2$/PEG by US irradiation might induce apoptosis in SDT, which is the same as PDT, it was inferred that apoptotic cell death through oxidative radicals in SDT might be less dominant in comparison with PDT.

In conclusion, the sonodynamic anti-tumor effect was strongly enhanced by water-dispersed $TiO_2$/PEG, and we confirmed that the mechanism of sonodynamic cytotoxicity differed from that of photodynamic cytotoxicity. $TiO_2$/PEG nanoparticles are approximately 50 nm in diameter. Particles of this size cannot cross the blood–brain barrier (BBB) theoretically [44]. However, these nanoparticles should accumulate in malignant glioma by transvascular delivery because the BBB is disrupted in malignant glioma [33,34,44]. Thus, $TiO_2$/PEG nanoparticles should be distributed only within the malignant glioma. In addition, magnetic resonance imaging-guided high intensity focus ultrasound for brain tumors has been developed in recent years [6–8]. By combining this method with accumulation of $TiO_2$/PEG, it may be possible to relieve damage to adjacent unaffected brain tissue. Although further investigations are needed, $TiO_2$/PEG nanoparticles can be a novel clinical material for sonodynamic therapy for malignant glioma.

## Acknowledgements

The authors thank the members of the TOTO Laboratory and Mrs. K. Tanaka and Mrs. S. Iino for helpful discussions and continuous support of the project. We also thank Ms. Yumiko Shinohe at the department of neurosurgery, graduate school of medicine and Hiroki Obara at the laboratory of biological engineering, graduate school of information science and technology, Hokkaido University for their excellent technical supports.

## References

[1] H. Inoue, Y. Kajimoto, M.A. Shibata, N. Miyoshi, N. Ogawa, S. Miyatake, Y. Otsuki, T. Kuroiwa, Massive apoptotic cell death of human glioma cells via a mitochondrial pathway following 5-aminolevulinic acid-mediated photodynamic therapy, J. Neurooncol. 83 (2007) 223–231.
[2] S. Karmakar, N.L. Banik, S.J. Patel, S.K. Ray, 5-Aminolevulinic acid-based photodynamic therapy suppressed survival factors and activated proteases for apoptosis in human glioblastoma U87MG cells, Neurosci. Lett. 415 (2007) 242–247.
[3] S.J. Madsen, E. Angell-Petersen, S. Spetalen, S.W. Carper, S.A. Ziegler, H. Hirschberg, Photodynamic therapy of newly implanted glioma cells in the rat brain, Lasers Surg. Med. 38 (2006) 540–548.
[4] S.J. Madsen, C.H. Sun, B.J. Tromberg, V.P. Wallace, H. Hirschberg, Photodynamic therapy of human glioma spheroids using 5-aminolevulinic acid, Photochem. Photobiol. 72 (2000) 128–134.
[5] C.H. Sibata, V.C. Colussi, N.L. Oleinick, T.J. Kinsella, Photodynamic therapy in oncology, Expert. Opin. Pharmacother. 2 (2001) 917–927.
[6] Z.R. Cohen, J. Zaubermann, S. Harnof, Y. Mardor, D. Nass, E. Zadicario, A. Hananel, D. Castel, M. Faibel, Z. Ram, Magnetic resonance imaging-guided focused ultrasound for thermal ablation in the brain: a feasibility study in a swine model, Neurosurgery 60 (2007) 593–600 (Discussion 600).
[7] N. McDannold, M. Moss, R. Killiany, D.L. Rosene, R.L. King, F.A. Jolesz, K. Hynynen, MRI-guided focused ultrasound surgery in the brain: tests in a primate model, Magn. Reson. Med. 49 (2003) 1188–1191.
[8] Z. Ram, Z.R. Cohen, S. Harnof, S. Tal, M. Faibel, D. Nass, S.E. Maier, M. Hadani, Y. Mardor, Magnetic resonance imaging-guided, high-intensity focused ultrasound for brain tumor therapy, Neurosurgery 59 (2006) 949–955 (Discussion 955–946).
[9] S. Dai, S. Hu, C. Wu, Apoptotic effect of sonodynamic therapy mediated by hematoporphyrin monomethyl ether on C6 glioma cells in vitro, Acta Neurochir. (Wien) 151 (2009) 1655–1661.

[10] J.H. Li, D.Y. Song, Y.G. Xu, Z. Huang, W. Yue, In vitro study of haematoporphyrin monomethyl ether-mediated sonodynamic effects on C6 glioma cells, Neurol. Sci. 29 (2008) 229–235.
[11] H. Abe, M. Kuroki, K. Tachibana, T. Li, A. Awasthi, A. Ueno, H. Matsumoto, T. Imakiire, Y. Yamauchi, H. Yamada, A. Ariyoshi, Targeted sonodynamic therapy of cancer using a photosensitizer conjugated with antibody against carcinoembryonic antigen, Anticancer Res. 22 (2002) 1575–1580.
[12] K. Hachimine, H. Shibaguchi, M. Kuroki, H. Yamada, T. Kinugasa, Y. Nakae, R. Asano, I. Sakata, Y. Yamashita, T. Shirakusa, Sonodynamic therapy of cancer using a novel porphyrin derivative, DCPH-P-Na(I), which is devoid of photosensitivity, Cancer Sci. 98 (2007) 916–920.
[13] Q. Liu, X. Wang, P. Wang, L. Xiao, Q. Hao, Comparison between sonodynamic effect with protoporphyrin IX and hematoporphyrin on sarcoma 180, Cancer Chemother. Pharmacol. 60 (2007) 671–680.
[14] K. Tachibana, N. Kimura, M. Okumura, H. Eguchi, S. Tachibana, Enhancement of cell killing of HL-60 cells by ultrasound in the presence of the photosensitizing drug Photofrin II, Cancer Lett. 72 (1993) 195–199.
[15] S. Umemura, N. Yumita, R. Nishigaki, K. Umemura, Mechanism of cell damage by ultrasound in combination with hematoporphyrin, Jpn. J. Cancer Res. 81 (1990) 962–966.
[16] N. Yumita, R. Nishigaki, I. Sakata, S. Nakajima, S. Umemura, Sonodynamically induced antitumor effect of 4-formyloximethylidene-3-hydroxy-2-vinyl-deuterio-porphynyl(IX)-6,7-dia spartic acid (ATX-S10), Jpn. J. Cancer Res. 91 (2000) 255–260.
[17] N. Yumita, R. Nishigaki, K. Umemura, S. Umemura, Hematoporphyrin as a sensitizer of cell-damaging effect of ultrasound, Jpn. J. Cancer Res. 80 (1989) 219–222.
[18] N. Yumita, K. Sasaki, S. Umemura, R. Nishigaki, Sonodynamically induced antitumor effect of a gallium-porphyrin complex, ATX-70, Jpn. J. Cancer Res. 87 (1996) 310–316.
[19] T. Ashikaga, M. Wada, H. Kobayashi, M. Mori, Y. Katsumura, H. Fukui, S. Kato, M. Yamaguchi, T. Takamatsu, Effect of the photocatalytic activity of TiO(2) on plasmid DNA, Mutat. Res. 466 (2000) 1–7.
[20] R. Cai, Y. Kubota, T. Shuin, H. Sakai, K. Hashimoto, A. Fujishima, Induction of cytotoxicity by photoexcited $TiO_2$ particles, Cancer Res. 52 (1992) 2346–2348.
[21] Y. Chihara, K. Fujimoto, H. Kondo, Y. Moriwaka, T. Sasahira, Y. Hirao, H. Kuniyasu, Anti-tumor effects of liposome-encapsulated titanium dioxide in nude mice, Pathobiology 74 (2007) 353–358.
[22] Y. Kubota, T. Shuin, C. Kawasaki, M. Hosaka, H. Kitamura, R. Cai, H. Sakai, K. Hashimoto, A. Fujishima, Photokilling of T-24 human bladder cancer cells with titanium dioxide, Br. J. Cancer 70 (1994) 1107–1111.
[23] E.A. Rozhkova, I. Ulasov, B. Lai, N.M. Dimitrijevic, M.S. Lesniak, T. Rajh, A high-performance nanobio photocatalyst for targeted brain cancer therapy, Nano Lett. 9 (2009) 3337–3342.
[24] J.W. Seo, H. Chung, M.Y. Kim, J. Lee, I.H. Choi, J. Cheon, Development of water-soluble single-crystalline TiO2 nanoparticles for photocatalytic cancer-cell treatment, Small 3 (2007) 850–853.
[25] J. Xu, Y. Sun, J. Huang, C. Chen, G. Liu, Y. Jiang, Y. Zhao, Z. Jiang, Photokilling cancer cells using highly cell-specific antibody-TiO(2) bioconjugates and electroporation, Bioelectrochemistry 71 (2007) 217–222.
[26] M.F. Dadjour, C. Ogino, S. Matsumura, S. Nakamura, N. Shimizu, Disinfection of Legionella pneumophila by ultrasonic treatment with $TiO_2$, Water Res. 40 (2006) 1137–1142.
[27] M. Kubo, R. Onodera, N. Shibasaki-Kitakawa, K. Tsumoto, T. Yonemoto, Kinetics of ultrasonic disinfection of *Escherichia coli* in the presence of titanium dioxide particles, Biotechnol. Prog. 21 (2005) 897–901.
[28] J. Wang, J. Wu, Z. Zhang, X. Zhang, Z. Pan, L. Wang, L. Xu, Sonocatalytic damage of bovine serum albumin (BSA) in the presence of nanometer anatase titanium dioxide ($TiO_2$), Ultrasound Med. Biol. 32 (2006) 147–152.
[29] B.K. Bernard, M.R. Osheroff, A. Hofmann, J.H. Mennear, Toxicology and carcinogenesis studies of dietary titanium dioxide-coated mica in male and female Fischer 344 rats, J. Toxicol. Environ. Health 29 (1990) 417–429.
[30] F. Bischoff, G. Bryson, Tissue reaction to fate of parenterally administered titanium dioxide. I. The intraperitoneal site in male Marsh-Buffalo mice, Res. Commun. Chem. Pathol. Pharmacol. 38 (1982) 279–290.
[31] E. Fabian, R. Landsiedel, L. Ma-Hock, K. Wiench, W. Wohlleben, B. van Ravenzwaay, Tissue distribution and toxicity of intravenously administered titanium dioxide nanoparticles in rats, Arch. Toxicol. 82 (2008) 151–157.
[32] S. Yamaguchi, H. Kobayashi, T. Narita, K. Kanehira, S. Sonezaki, Y. Kubota, S. Terasaka, Y. Iwasaki, Novel photodynamic therapy using water-dispersed TiO-polyethylene glycol compound: evaluation of antitumor effect on glioma cells and spheroids in vitro, Photochem. Photobiol. 86 (2010) 964–971.
[33] H. Sarin, A.S. Kanevsky, H. Wu, K.R. Brimacombe, S.H. Fung, A.A. Sousa, S. Auh, C.M. Wilson, K. Sharma, M.A. Aronova, R.D. Leapman, G.L. Griffiths, M.D. Hall, Effective transvascular delivery of nanoparticles across the blood–brain tumor barrier into malignant glioma cells, J. Transl. Med. 6 (2008) 80.
[34] K.E. Schlageter, P. Molnar, G.D. Lapin, D.R. Groothuis, Microvessel organization and structure in experimental brain tumors: microvessel populations with distinctive structural and functional properties, Microvasc. Res. 58 (1999) 312–328.
[35] W. Hiraoka, H. Honda, L.B. Feril Jr., N. Kudo, T. Kondo, Comparison between sonodynamic effect and photodynamic effect with photosensitizers on free radical formation and cell killing, Ultrason. Sonochem. 13 (2006) 535–542.
[36] D. Kessel, J. Lo, R. Jeffers, J.B. Fowlkes, C. Cain, Modes of photodynamic vs. sonodynamic cytotoxicity, J. Photochem. Photobiol. B 28 (1995) 219–221.
[37] J. Yang, S. Mei, J.M.F. Ferreira, Hydrothermal synthesis of nanosized titania powders: influence of tetraalkyl ammonium hydroxides on particle characteristics, J. Am. Ceram. Soc. 84 (2001) 1696–1702.
[38] K. Kanehira, T. Banzai, C. Ogino, N. Shimizu, Y. Kubota, S. Sonezaki, Properties of $TiO_2$-polyacrylic acid dispersions with potential for molecular recognition, Colloids Surf. B Biointerfaces 64 (2008) 10–15.
[39] F. Denizot, R. Lang, Rapid colorimetric assay for cell growth survival. Modifications to the tetrazolium dye procedure giving improved sensitivity and reliability, J. Immunol. Methods 89 (1986) 271–277.
[40] L.B. Feril Jr., T. Kondo, Z.G. Cui, Y. Tabuchi, Q.L. Zhao, H. Ando, T. Misaki, H. Yoshikawa, S. Umemura, Apoptosis induced by the sonomechanical effects of low intensity pulsed ultrasound in a human leukemia cell line, Cancer Lett. 221 (2005) 145–152.
[41] A. Fujishima, T.N. Rao, D.A. Tryk, Titanium dioxide photocatalysis, J. Photochem. Photobiol. C 1 (2000) 1–21.
[42] Y. Higuchi, Chromosomal DNA fragmentation in apoptosis and necrosis induced by oxidative stress, Biochem. Pharmacol. 66 (2003) 1527–1535.
[43] I. Rosenthal, J.Z. Sostaric, P. Riesz, Sonodynamic therapy – a review of the synergistic effects of drugs and ultrasound, Ultrason. Sonochem. 11 (2004) 349–363.
[44] W.M. Pardridge, Drug and gene delivery to the brain: the vascular route, Neuron 36 (2002) 555–558.

# SHP-2/*PTPN11* mediates gliomagenesis driven by *PDGFRA* and *INK4A/ARF* aberrations in mice and humans

Kun-Wei Liu,[1,2] Haizhong Feng,[1,2] Robert Bachoo,[3] Andrius Kazlauskas,[4] Erin M. Smith,[5] Karen Symes,[5] Ronald L. Hamilton,[2] Motoo Nagane,[6] Ryo Nishikawa,[7] Bo Hu,[1,8] and Shi-Yuan Cheng[1,2]

[1]University of Pittsburgh Cancer Institute and [2]Department of Pathology, University of Pittsburgh School of Medicine, Pittsburgh, Pennsylvania, USA. [3]Department of Internal Medicine, University of Texas Southwestern Medical Center, Dallas, Texas, USA. [4]Schepens Eye Research Institute and Harvard Medical School, Boston, Massachusetts, USA. [5]Department of Biochemistry, Boston University School of Medicine, Boston, Massachusetts, USA. [6]Department of Neurosurgery, Kyorin University Faculty of Medicine, Tokyo, Japan. [7]Department of Neurosurgery, Saitama Medical University, Saitama-ken, Japan. [8]Department of Medicine, University of Pittsburgh School of Medicine, Pittsburgh, Pennsylvania, USA.

**Recent collaborative efforts have subclassified malignant glioblastomas into 4 clinical relevant subtypes based on their signature genetic lesions. Platelet-derived growth factor receptor α (*PDGFRA*) overexpression is concomitant with a loss of cyclin-dependent kinase inhibitor 2A (*CDKN2A*) locus (encoding P16INK4A and P14ARF) in a large number of tumors within one subtype of glioblastomas. Here we report that activation of PDGFRα conferred tumorigenicity to *Ink4a/Arf*-deficient mouse astrocytes and human glioma cells in the brain. Restoration of p16INK4a but not p19ARF suppressed PDGFRα-promoted glioma formation. Mechanistically, abrogation of signaling modules in PDGFRα that lost capacity to bind to SHP-2 or PI3K significantly diminished PDGFRα-promoted tumorigenesis. Furthermore, inhibition of SHP-2 by shRNAs or pharmacological inhibitors disrupted the interaction of PI3K with PDGFRα, suppressed downstream AKT/mTOR activation, and impaired tumorigenesis of *Ink4a/Arf*-null cells, whereas expression of an activated PI3K mutant rescued the effect of SHP-2 inhibition on tumorigenicity. PDGFRα and PDGF-A are co-expressed in clinical glioblastoma specimens, and such co-expression is linked with activation of SHP-2/AKT/mTOR signaling. Together, our data suggest that in glioblastomas with *Ink4a/Arf* deficiency, overexpressed PDGFRα promotes tumorigenesis through the PI3K/AKT/mTOR-mediated pathway regulated by SHP-2 activity. These findings functionally validate the genomic analysis of glioblastomas and identify SHP-2 as a potential target for treatment of glioblastomas.**

## Introduction

Human gliomas account for the most common and malignant tumors in the CNS (1). Despite intensive treatments including maximal surgical resection, combined with radiotherapy and concurrent or adjuvant chemotherapies, median survival time of patients with high-grade glioblastoma multiforme (GBM) remains 14–16 months after diagnosis (1, 2). Recently, coordinated genomic analyses of a large cohort of clinical GBM specimens identified frequent co-alterations of genes in 3 core pathways — the P53, retinoblastoma (RB), and receptor tyrosine kinase (RTK) pathways — that are crucial in gliomagenesis (3). Notably, the gene encoding platelet-derived growth factor receptor α (PDGFRα) is amplified in approximately 13% of total GBMs analyzed, and deletion of the tumor suppressor cyclin-dependent kinase inhibitor 2A (*CDKN2A*) locus is frequently found in these PDGFRα-amplified GBMs (3, 4). However, to our knowledge, studies have not been conducted to determine whether these genetic aberrations act in concert to promote gliomagenesis, or to determine the underlying mechanisms of PDGFRα-stimulated tumorigenesis.

The homozygous deletion of the *CDKN2A* locus at chromosome 9p21, which eliminates both *INK4A* and *ARF* genes (encoding P16INK4A and P14ARF, respectively), concomitantly deregulates 2 of the major tumor suppressor pathways, the RB and P53 pathways (5). Mice lacking the *Cdkn2a* locus develop spontaneous tumors and are more prone to carcinogenesis (6). Whereas no spontaneous tumors are found in the brain of *Ink4a/Arf*-deficient mice, astrocytes and neural stem cells (NSCs) from these mice form high-grade gliomas in the brain upon EGFR activation (7). Additionally, K-Ras activation has been shown to cooperate with loss of *Ink4a* and *Arf* in mouse astrocytes (mAsts) or neural progenitor cells to generate GBMs (8).

PDGFRα is a RTK that elicits a variety of biological activities such as cell proliferation and migration via stimulation by its ligand dimers, PDGF-AA, -AB, -BB, -CC, and -DD. Activated PDGFRα associates via the autophosphorylated tyrosine (p-Y) residues at its cytoplasmic domain to various downstream SH2 domain–containing signaling molecules, including SRC family kinases (SFKs), phosphotyrosine phosphatase SHP-2, PI3K, and PLCγ (9, 10). Mice deficient in PDGFRα or PDGF-A or engineered to separately express PDGFRα with mutations of the individual p-Y sites show alterations in cellular behavior and embryo development (9, 11). In particular, PI3K has been identified as the major effector of PDGFRα signaling in vitro and in vivo (10, 12, 13). SFKs and PLCγ contribute to some but not all PDGFRα functions (10, 12–14), whereas SHP-2 is not required for cell survival during Xenopus embryogenesis (12). However, contributions of each of these signaling modules to glioma formation have not to our knowledge been demonstrated.

**Conflict of interest:** The authors have declared that no conflict of interest exists.
**Citation for this article:** *J Clin Invest.* 2011;121(3):905–917. doi:10.1172/JCI43690.

Activation of PDGFRα signaling has been observed in human gliomas. In clinical glioma specimens, PDGFRα and PDGF-A are overexpressed in tumor cells, while PDGFRβ is only expressed in endothelial and peri-endothelial compartments (15). PDGF-B, which binds to both PDGFRα and PDGFRβ, is an oncoprotein that causes glioma formation in the brain (16). Loss of *Ink4a/Arf* in mAsts enhances PDGF-B–initiated gliomagenesis and tumor progression in the brain (16). Specific activation of PDGFRα signaling by infusion of PDGF-A proteins, which only bind to PDGFRα in PDGFRα-positive type B NSCs in the subventricular zone (SVZ), leads to glioma-like growth of these cells in adult brain (17). However, how the activation of PDGFRα signaling causes glioma formation and whether co-alteration of tumor suppressor pathways is required in PDGFRα-mediated gliomagenesis have not been directly shown. In this study, we determined the synergistic impact of *PDGFRA* overexpression and *INK4A/ARF* deletion on gliomagenesis in mAsts and human glioma cells. We then used genetic and pharmacological approaches targeting individual downstream signaling enzymes to examine which specific signaling pathway(s) emanating from PDGFRα are critical in tumorigenesis. Furthermore, we confirmed our observations in clinical glioma specimens that co-overexpress PDGFRα and PDGF-A.

## Results

*Overexpression of PDGFRα and/or PDGF-A confers tumorigenicity to Ink4a/Arf$^{-/-}$ mAsts.* To determine whether activation of PDGFRα signaling in *Ink4a/Arf*$^{-/-}$ mAsts leads to gliomagenesis in the brain, we overexpressed PDGFRα and/or its ligand PDGF-A chain in a retroviral vector containing an IRES-GFP in *Ink4a/Arf*$^{-/-}$ mAsts (Figure 1A). The impact of PDGFRα/PDGF-A overexpression on the growth and survival of these cells in vitro was moderate (Supplemental Figure 1, A and B; supplemental material available online with this article; doi:10.1172/JCI43690DS1). However, when these cells were separately transplanted into the flanks of mice, significant s.c. tumor growth was evident in mice that separately received *Ink4a/Arf*$^{-/-}$ mAsts expressing PDGFRα, PDGF-A, or PDGFRα/PDGF-A (with the receptor and ligand co-expressed in the same cell to create an autocrine signaling), whereas minimal or no tumor formation was seen in control mice that received *Ink4a/Arf*$^{-/-}$ mAsts expressing GFP (Figure 1B). To determine tumorigenicity of these cells in the brain, various mAsts were separately implanted into the brain of mice. Notably, mice that received GFP mAsts did not show active tumor growth up to 42 days after implantation, while PDGFRα, PDGF-A, and PDGFRα/PDGF-A mAsts started to form tumors in the brain as early as 8–11 days and the majority of tumors reached a volume of approximately 25 to 30 $mm^3$ in 25–35 days. Moreover, mice that separately received PDGFRα- or PDGF-A–expressing mAsts survived up to 2 months after implantation. On the other hand, all mice that received autocrine PDGFRα/PDGF-A–expressing mAsts developed large and invasive tumors by 20 days, with an average survival time of 25 days after implantation. As shown in Figure 1, C–L, significantly larger and highly invasive gliomas formed in the brains of mice that received *Ink4a/Arf*$^{-/-}$ mAsts overexpressing PDGFRα, PDGF-A, or PDGFRα/PDGF-A, whereas only small tumor lesions were found in the brain of mice that received control mAsts. Significantly, an approximately 10-fold increase in the cell proliferation index was found in gliomas derived from PDGFRα-activated mAsts compared with control tumors (Figure 1, M–R), whereas an approximately 10-fold decrease of cell apoptosis was seen in PDGFRα/PDGF-A–expressing tumors (Figure 1S). Of note, in established s.c. or brain tumors, exogenous expression of PDGFRα or PDGF-A was maintained at the end of the experiments (Supplemental Figure 1, C–K, and data not shown). Taken together, these results indicate that expression of PDGFRα and/or PDGF-A confers tumorigenicity to *Ink4a/Arf*-deficient mAsts in the brain.

To further characterize the tumors derived from *Ink4a/Arf*$^{-/-}$ PDGFRα mAsts, we examined molecular markers of various cell lineages in the CNS development. As shown in Figure 2, tumors derived from PDGFRα-expressing mAsts were highly positive for the neural progenitor marker nestin, which was distributed along the processes of individual cells (Figure 2, A and B). As expected, most of tumor cells showed expression of the progenitor/mature astrocyte marker GFAP (Figure 2, C and D) but were negative for the neuronal marker class III β-tubulin (TUJ1) (Figure 2, E and F). Significantly, NG2, an oligodendrocyte progenitor cell marker (18), was expressed in a population of tumor cells that were actively invading the surrounding brain parenchyma, whereas the core of the tumor mass showed relatively low NG2 expression (Figure 2, G and H). In contrast, control tumors derived from *Ink4a/Arf*$^{-/-}$ GFP mAsts lacked nestin or NG2 expression (data not shown). In addition, tumors derived from *Ink4a/Arf*$^{-/-}$ PDGFRα mAsts showed negative staining for oligodendrocyte type 2 astrocyte progenitor marker A2B5 and an oligodendrocyte marker CNPase (data not shown). Notably, brain tumors derived from *Ink4a/Arf*$^{-/-}$ PDGFRα/PDGF-A mAsts (data not shown) displayed similar IHC features to tumors derived from *Ink4a/Arf*$^{-/-}$ PDGFRα mAsts, suggesting that similar dedifferentiation events also occurred in autocrine PDGFRα/PDGF-A–co-expressing tumors.

*Exogenous expression of PDGF-A enhances tumorigenicity of Ink4a/Arf-null but not WT Ink4a/Arf human glioma cells in the brain.* Next, we used 4 human glioma cell lines that were either *INK4A/ARF* null (LN444 and LN443) or WT *INK4A/ARF* (LN-Z308 and LN319; Figure 3A) (19) and exogenously expressed PDGF-A in these glioma cells that express endogenous PDGFRα (Figure 3B). In vitro, expression of PDGF-A in *INK4A/ARF*-null LN444 cells significantly enhanced their capacity of anchorage-independent growth in soft agar, whereas a minimal effect was seen in WT *INK4A/ARF* LN-Z308 and LN319 cells (Figure 3C). When various glioma cells were separately implanted into the brain or the flanks of mice, PDGF-A expression markedly enhanced tumor growth and invasion of *INK4A/ARF*-null LN444 and LN443 glioma cells, while minimal impact of PDGF-A expression on tumorigenesis or invasion was seen in WT *INK4A/ARF* LN-Z308 and LN319 cells in both anatomic sites (Figure 3, D–K, and Supplemental Figure 2). Mice received LN444/PDGF-A cells in the brain had tumor onset as early as 35 days, while mice with LN443/PDGF-A cells developed invasive intracranial tumor 25–30 days after implantation. In contrast, LN444 and LN443 parental cells only formed small tumor lesions in the brain up to 2–3 months following implantation. Mice that received LN444/PDGF-A cells survived for 75–80 days, while most of the mice that received LN443/PDGF-A cells lived up to 3 months after implantation. On the other hand, no significant brain tumor growth was found 2–3 months after implantation in mice that received LN-Z308/PDGF-A or LN319/PDGF-A cells. Thus, consistent with our findings in the *Ink4a/Arf*$^{-/-}$ mAsts, these data indicate that PDGFRα/PDGF-A signaling enhances in vivo tumor growth and invasion of human glioma cells deficient in *INK4A/ARF*.

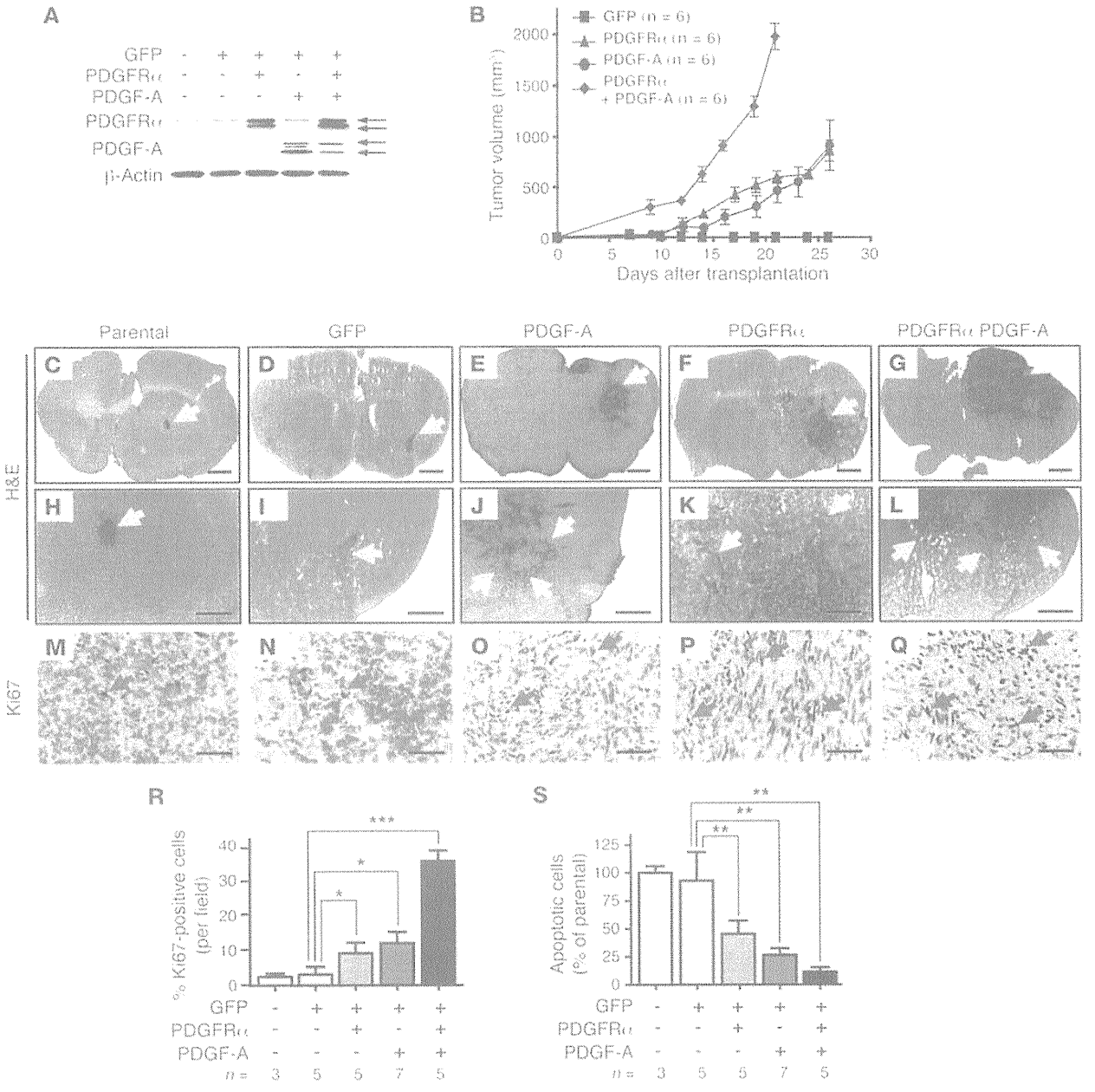


**Figure 1**

PDGFRα and/or PDGF-A overexpression promotes tumorigenesis of *Ink4a/Arf*$^{-/-}$ mAsts. (**A**) IB analysis of exogenous expression of PDGFRα and/or PDGF-A in mAsts. Arrows indicate PDGFRα and PDGF-A proteins run as doublet bands. β-Actin was used as a loading control. (**B**) Tumor growth of various mAsts s.c. Data are shown as mean ± SD. (**C–L**) Representative H&E staining images of various brain sections from 2 independent experiments with at least 3–5 mice per group with similar results. Brains were harvested 25–30 days after transplantation for **C–F** and 20 days after transplantation for **G**. Scale bars: 1 mm (**C–G**); 200 μm (**H–L**). (**M–Q**) Ki-67 staining of the corresponding brain sections in (**C–G**). Yellow arrows indicate tumor mass or invading tumor cells. Red arrows indicate Ki-67–positive cells. Scale bars: 50 μm. (**R** and **S**) Quantification of Ki-67 staining (**R**) and TUNEL staining (**S**) of various brain sections. Data are presented as percentage to parental controls (mean ± SD). *n*, the number of mice used for each group. $^{*}P < 0.05$; $^{**}P < 0.01$; $^{***}P < 0.001$.

*p16INK4a but not p19ARF attenuates the PDGFRα-promoted tumorigenesis of Ink4a/Arf-deficient mAsts and human glioma cells.* To investigate whether re-expression p16INK4a or p19ARF is able to abrogate the enhanced tumorigenicity in *Ink4a/Arf*$^{-/-}$ mAsts, we separately expressed these 2 tumor suppressors in mAsts (Figure 4A). Surprisingly, re-expression of p16INK4a but not p19ARF alone in *Ink4a/Arf*$^{-/-}$ mAsts suppressed soft agar growth of PDGFRα-expressing mAsts stimulated by PDGF-A (Figure 4B). Consistently, enforced restoration of p16INK4a in *Ink4a/Arf*$^{-/-}$ mAsts significantly inhibited tumorigenesis of PDGFRα/PDGF-A–overexpressing mAsts in the mouse brain (Figure 4C). To further demonstrate the cooperative effect of PDGFRα activation and loss of *Ink4a* on tumorigenesis, we knocked down endogenous p16INK4a using shRNAs targeting *CDKN2A* in

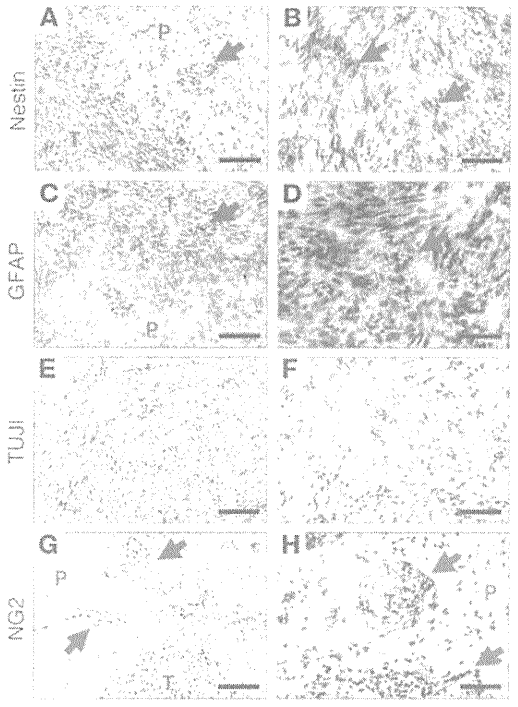


**Figure 2**
Tumors derived from *Ink4a/Arf*$^{-/-}$ PDGFRα mAsts express markers of neural progenitor cells. Representative images of IHC staining using antibodies against nestin (**A** and **B**), GFAP (**C** and **D**), βIII-tubulin (**E** and **F**), and NG2 (**G** and **H**). Arrows indicate positive staining of various markers. T, tumor mass; P, normal brain parenchyma. Scale bars: 100 μm (**A**, **C**, **E**, and **G**); 50 μm (**B**, **D**, **F**, and **H**).

WT *INK4A/ARF* LN319 cells. As shown in Figure 4D, significant inhibition of P16INK4A without affecting P14ARF expression by 2 separate shRNAs in LN319 cells resulted in a marked increase in colony formation in soft agar. Since p16INK4a inhibits CDK4/6, which inactivates RB by phosphorylation, and since p19ARF (or P14ARF) targets MDM2, which suppresses p53 (5), we thus examined responses of modulating CDK4/6 and p53 in these cells. As shown in Figure 4E, inhibition of phosphorylation of RB, the direct downstream target of CDK4/6 by CDK4/6 inhibitor PD0332991 (20), markedly reduced PDGF-A–stimulated cell growth of *Ink4a/Arf*-deficient mAsts and LN444 cells in soft agar, which suggests that the tumorigenic effect of PDGFRα signaling is dependent on CDK4/6 inactivation of RB proteins (p-RB). Since we did not observe any tumor-suppressing effect of p19ARF on *Ink4a/Arf*$^{-/-}$ PDGFRα-expressing mAsts (Figure 4B), we asked whether the downstream p53 protein was functional in these cells. When *Ink4a/Arf*$^{-/-}$ and *Ink4a/Arf*$^{-/-}$ p19ARF mAsts were treated with cisplatin (21), p53 expression was strongly induced in *Ink4a/Arf*$^{-/-}$ PDGFRα/p19ARF-expressing mAsts but only moderately induced in *Ink4a/Arf*$^{-/-}$ PDGFRα-expressing mAsts (Supplemental Figure 3A). The mAsts expressing p19ARF were more sensitive to cisplatin inhibition of cell survival than those without p19ARF expression, indicating that p19ARF-upregulated p53 in *Ink4a/Arf*$^{-/-}$ PDGFRα-expressing mAsts rendered sensitivity to cisplatin inhibition (Supplemental Figure 3B). Collectively, these data show that p16INK4a but not p19ARF suppresses the tumorigenesis promoted by PDGFRα/PDGF-A signaling, suggesting a cooperative effect of PDGFRα activation and p16INK4a inhibition during gliomagenesis. Additionally, p19ARF loss might be required for tumor survival in certain circumstances such as in the presence of DNA-damaging agents.

*PDGFRα-enhanced tumorigenicity is mediated by SHP-2 and PI3K signaling.* Previous studies using genetic and biochemical approaches have defined the roles of signaling molecules in PDGFRα-mediated cellular functions by specific tyrosine-to-phenylalanine (Y-to-F) mutations (Figure 5A) (10, 12, 13). To investigate the impact of these PDGFRα mutations on tumorigenesis, we separately expressed WT PDGFRα or various PDGFRα mutants in *Ink4a/Arf*$^{-/-}$ mAsts. The PDGFRα mutant R627 (PDGFRα-R627) that harbors a lysine-to-arginine (K-to-R) mutation was included as a "receptor kinase–dead" control. As shown in Figure 5B, stimulation of WT PDGFRα by PDGF-A resulted in autophosphorylation of the receptor and promoted phosphorylation of downstream signaling molecules Erk1/2 and Akt, whereas there was an undetectable receptor tyrosine autophosphorylation in PDGFRα-R627 (Figure 5B). PDGFRα Y-to-F mutations at Y572 and Y574 (PDGFRα-F572/74; for SFK binding), Y1018 (PDGFRα-F1018; for PLCγ binding), and Y988 (PDGFRα-F988) did not result in a significant decrease in p-Akt and p-Erk levels in response to PDGF-A stimulation (Figure 5B). Moreover, the mutation at Y731 and Y742 (PDGFRα-F731/42; for PI3K binding) led to a marked decrease in PDGF-A–stimulated p-Akt and p-Erk1/2 levels (Figure 5B). In agreement with a previous report (22), p-Erk1/2 was markedly reduced in PDGF-A–stimulated mAsts expressing PDGFRα-F720 (Y-to-F mutation at Y720; for SHP-2 binding), compared with WT PDGFRα mAsts (Figure 5B). Interestingly, p-Akt levels were also attenuated in PDGFRα-F720 cells.

Next, we determined the impact of these Y-to-F mutations on PDGFRα-promoted cell transformation of *Ink4a/Arf*$^{-/-}$ mAsts in vitro. As shown in Figure 5C, mAsts expressing WT PDGFRα and PDGFRα-F572/74, PDGFRα-F988, and PDGFRα-F1018 PDGFRα mutants showed similar capability of anchorage-independent growth in soft agar. In contrast, expression of PDGFRα-R627, PDGFRα-F731/42, or PDGFRα-F720 instead of WT PDGFRα significantly abrogated the capacity of mAsts to form colonies in soft agar (Figure 5, C and D), indicating that PI3K and SHP-2 signaling were critical for cell transformation in vitro. When various *Ink4a/Arf*$^{-/-}$ mAsts were separately implanted into the brains of mice, PDGFRα-R627, PDGFRα-F731/42, PDGFRα-F720, and PDGFRα-F988 significantly impaired PDGFRα-promoted tumorigenesis and invasion compared with WT PDGFRα (Figure 6, B, C, E, and F, compared with Figure 6A). However, mAsts expressing PDGFRα-F572/74 or PDGFRα-F1018 displayed tumorigenicity comparable to WT PDGFRα tumors (Figure 6, D and G, compared to 6A), but showed markedly reduced tumor invasion compared with the tumors derived from mAsts expressing WT PDGFRα (Figure 6, K and N, compared with 6H). Higher-magnification images of PDGFRα-R627, PDGFRα-F731/42, and PDGFRα-F720 mutants (Figure 6, I, J, and L) further illustrated that these mutations significantly negated the enhanced tumorigenicity conferred by PDGFRα activation, leading to the formation of tumors similar in volume and invasiveness to those seen in GFP-expressing mAst tumors (Figure 1, D and I). Moreover, PDGFRα-F731/42 and PDGFRα-F720 tumors showed a significantly decreased cell proliferation (Figure 6, O and P) and increased apoptosis

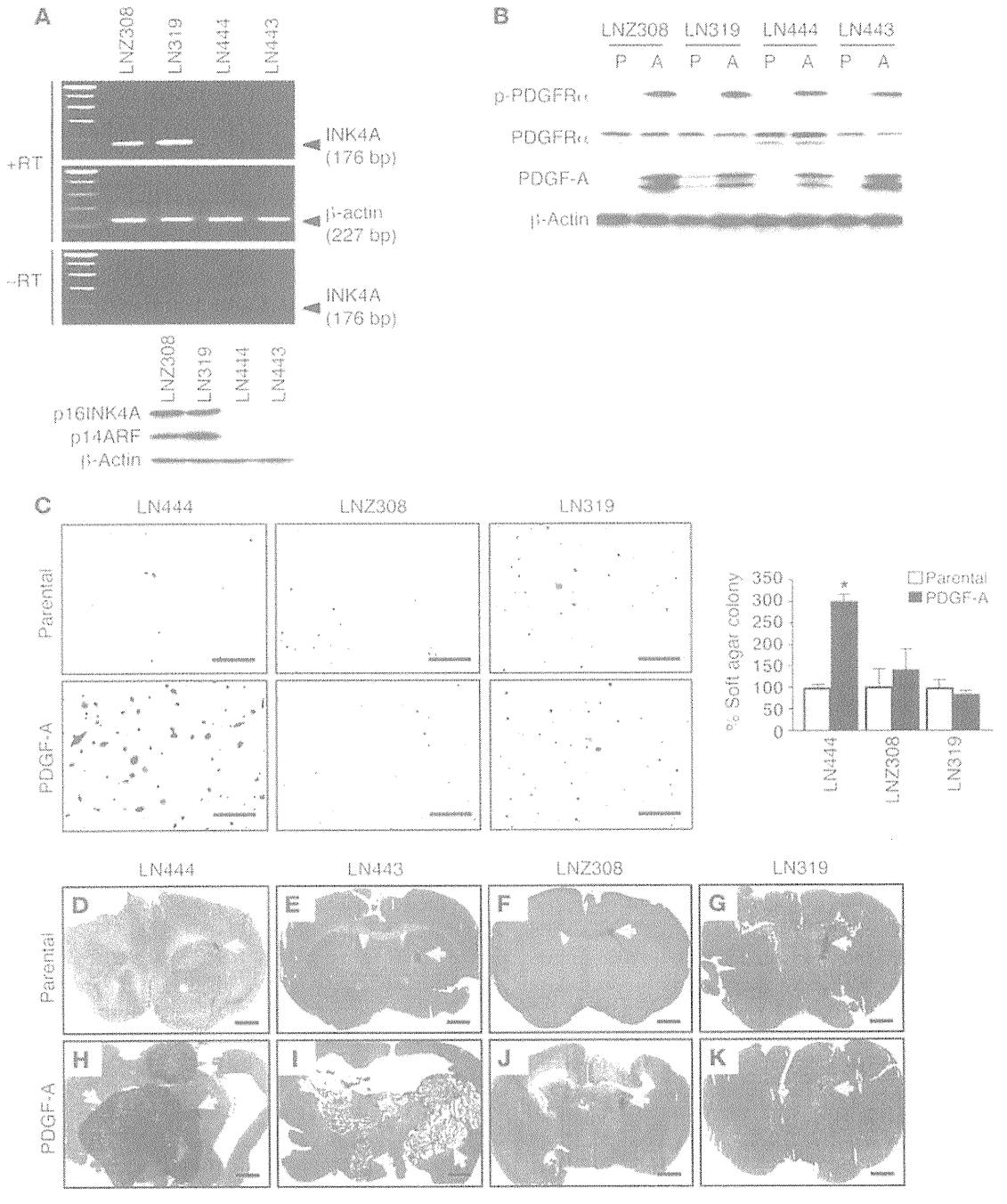


**Figure 3**

PDGF-A overexpression enhances tumorigenesis of *INK4A/ARF*-deficient but not WT *INK4A/ARF* human glioma cells. (**A**) RT-PCR (top) and IB analyses (bottom) of *INK4A/ARF*-deficient LN444 and LN443 and WT *INK4A/ARF* LN-Z308 and LN319 human glioma cells. (**B**) IB analysis of PDGF-A overexpression in glioma cells with endogenous PDGFRα expression. PDGFRα was phosphorylated at tyrosine residues in PDGF-A–expressing cells, but not in parental cells that have no detectable PDGF-A. P, parental cells; A, PDGF-A–overexpressing cells. β-Actin was used as a loading control in both **A** and **B**. (**C**) Representative images (left) and quantification (right) of anchorage-independent growth of various glioma cells in soft agar. Scale bars: 1 mm. Data are presented as percentage of the respective parental cells (mean ± SD). $^*P < 0.001$, Student's *t* test. (**D**–**K**) Representative H&E-stained images of various brain sections from 2 independent experiments with 3–5 mice per group with similar results. Brains were harvested 50–55 days (**D** and **H**), 75–80 days (**E** and **I**), and 45–50 days (**F**, **G**, **J**, and **K**) after transplantation. Arrows indicate gliomas formed in the brain. Scale bar: 1 mm.

(Figure 6, Q and R), whereas PDGFRα-F572/74, PDGFRα-F988, and PDGFRα-F1018 tumors exhibited moderate or minimal impacts on cell proliferation and survival compared with WT PDGFRα tumors. Conversely, retention of any 1 of the 5 signaling modules (Y731/42, Y572/74, Y720, Y988, and Y1018 PDGFRα mutants) (10) was insufficient to rescue the abolished tumorigenesis in the brain (data not shown). Taken together, these data indicate that ablation of PDGFRα association with

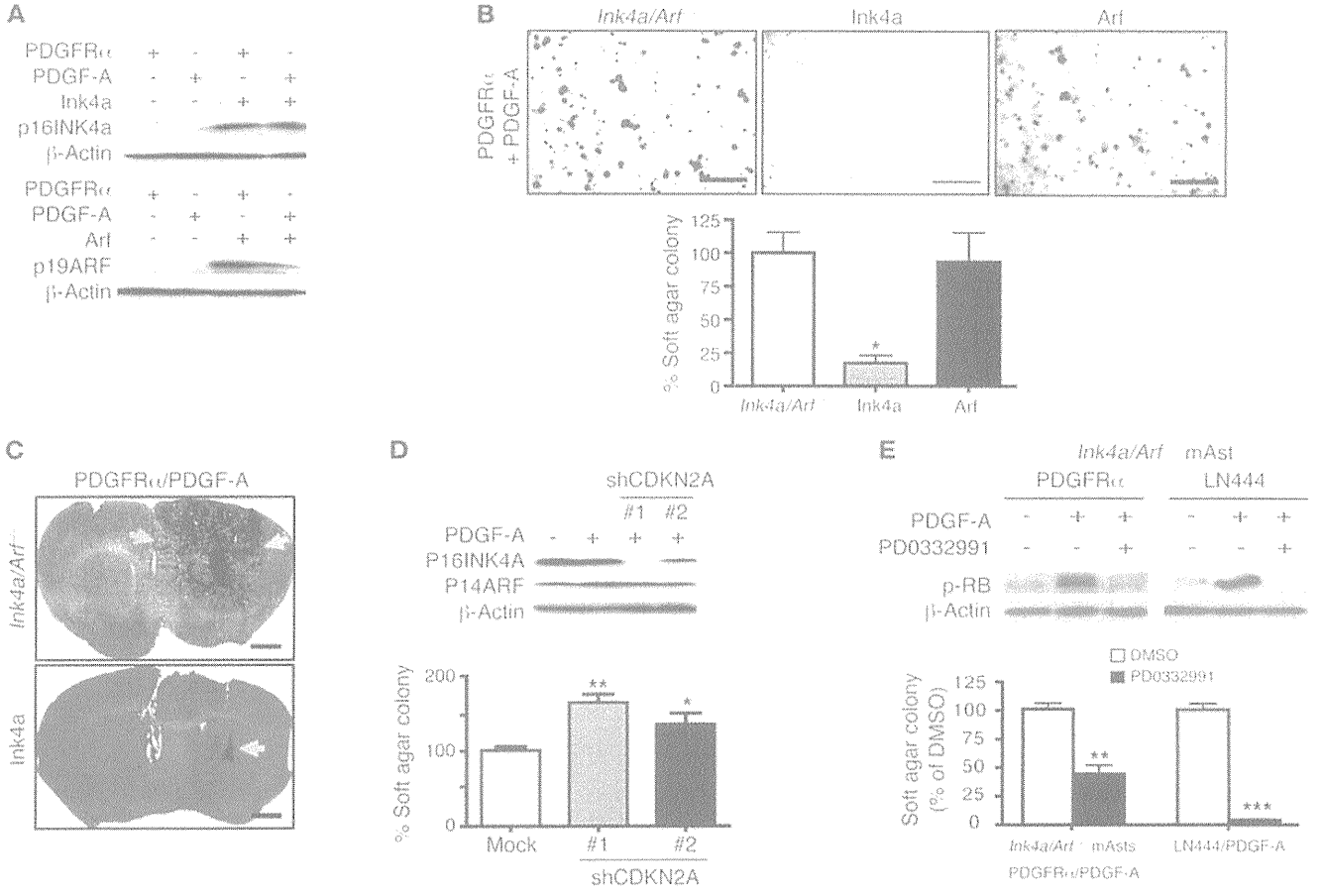


**Figure 4**

Re-expression of p16INK4a but not p19ARF suppresses the tumorigenesis of mAsts expressing PDGFRα/PDGF-A. (**A**) IB analyses of re-expression of p16INK4a or p19ARF in PDGFRα- or PDGF-A–overexpressing *Ink4a/Arf*$^{-/-}$ mAsts. (**B**) Top: Anchorage-independent growth of p16INK4a- or p19ARF-expressing mAsts. Scale bars: 1 mm. Bottom: Quantification of soft agar assays. Data are presented as mean ± SD. $^{*}P < 0.05$. (**C**) Representative H&E staining images of various brain sections from 2 independent experiments with 3–5 mice per group with similar results. Brains were harvested 18–22 days after implantation. Mice that received either type of cell displayed similar tumor onset and survival times as mice in Figure 1. Scale bars: 1 mm. (**D**) Anchorage-independent growth of WT *INK4A/ARF* LN319 cells transfected with shCDKN2A in soft agar. Top: IB analysis. Bottom: Quantification of soft agar assays. Two stable cell clones (#1 and #2) with different efficiencies of P16INK4A knockdown were used. Data are mean ± SD. (**E**) Soft agar growth of *Ink4a/Arf*-deficient mAsts and LN444 cells treated with PD0332991. Top: IB analysis. Bottom: Quantification of soft agar assays. β-Actin was used as a loading control in all IB experiments. Data are presented as mean ± SD and are representative of 2 independent experiments. $^{*}P < 0.05$; $^{**}P < 0.01$; $^{***}P < 0.001$.

SHP-2 or PI3K abrogates tumorigenicity of *Ink4a/Arf*$^{-/-}$ mAsts expressing PDGFRα, whereas individual association of PI3K, SHP-2, SFK, or PLCγ with the RTK was insufficient to elicit the full spectrum of tumor-promoting effects of PDGFRα.

*Pharmacological inhibition of SHP-2 or PI3K abrogates PDGFRα-promoted tumorigenesis of Ink4a/Arf-deficient mAsts and human glioma cells.* We further investigated whether inhibition of SHP-2 and PI3K activities by pharmacological approaches suppresses tumorigenicity of PDGFRα/PDGF-A–expressing *Ink4a/Arf*$^{-/-}$ mAst and LN444 cells. To this end, we exploited several pharmacological inhibitors against PI3K (LY294002), SHP-2 (PHPS-1 and NSC87877) (23), and SFKs (SU6656, and PP2). As shown in Figure 7, LY294002 inhibited PDGF-A–induced phosphorylation of Akt at 10 μM in mAsts and 5 μM in LN444 glioma cells, whereas Erk1/2 phosphorylation was unaffected by LY294002 treatment in both types of cells (Figure 7, A and B). Of note, a modest decrease was observed in p-Erk1/2 levels in mAsts treated with 20 μM LY294002 (Figure 7A). At a concentration of 100 μM (23), both PHPS-1 and NSC87877 significantly inhibited p-Erk1/2, a direct downstream target of SHP-2, in mAsts and LN444 cells (Figure 7, A and B). Next, we examined the impact of the pharmacological interventions of these signaling enzymes on in vitro cell transformation and found that 10 μM LY294002, which had no effect on Erk1/2 activation, suppressed soft agar growth of PDGFRα-expressing mAsts stimulated by PDGF-A (Figure 7A) and PDGF-A–expressing LN444 cells (Figure 7B). Similarly, 100 μM of either PHPS-1 or NSC87877 ablated PDGFRα-stimulated, anchorage-independent growth in soft agar but only had a minimal effect on the cell survival and caspase-3 activation of both PDGFRα/PDGF-A–expressing mAsts and LN444 cells in culture (Supplemental Figure 4, A and B). In contrast, 2 SFK inhibitors, SU6656 and PP2 each at 5-μM concentration, only showed a modest impact on tumorigenesis of these cells (Figure 7, A and B). Additionally, the MEK inhibitor PD98059 at 10 μM, which suppressed PDGF-A–induced

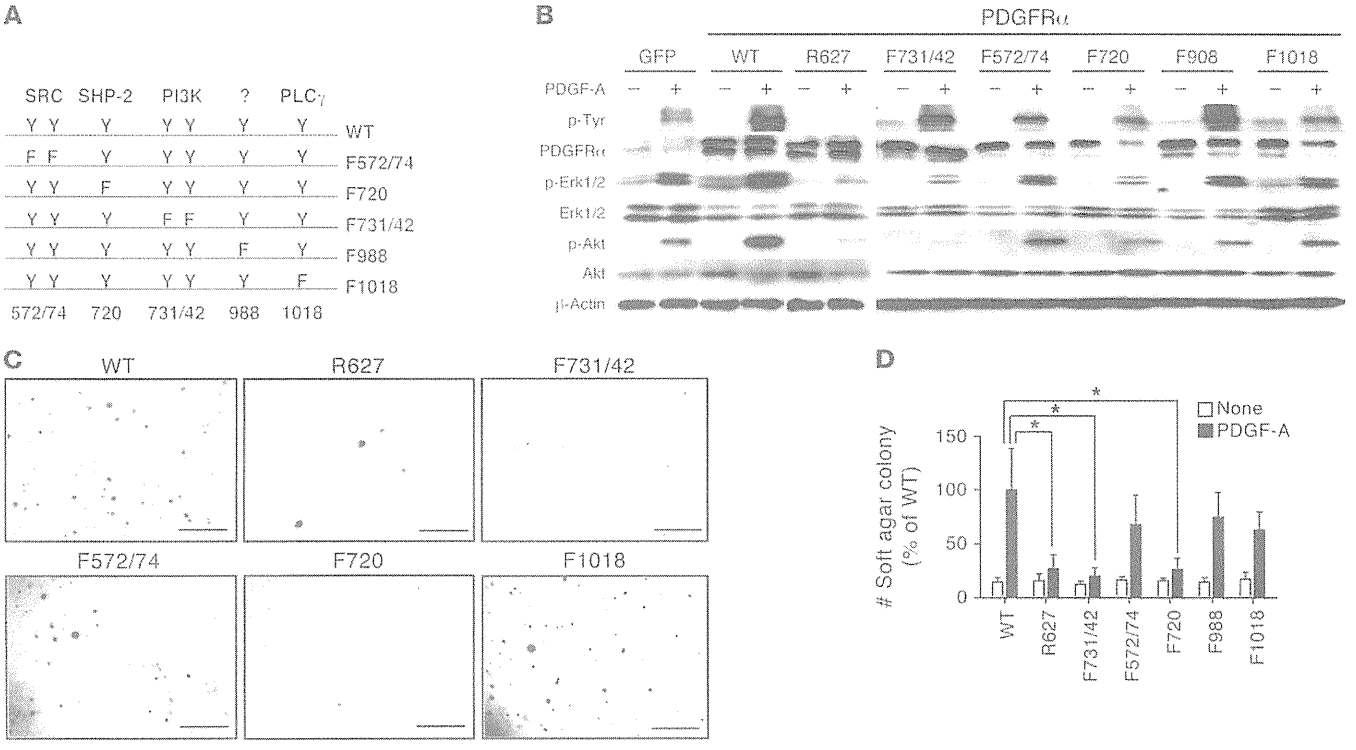


**Figure 5**
Impacts of PDGFRα mutations on downstream signaling of PDGFRα and anchorage-independent growth in soft agar of *Ink4a/Arf*$^{-/-}$ mAsts. (**A**) Schematics of various PDGFRα mutants. (**B**) IB analyses of PDGF-A–stimulated *Ink4a/Arf*$^{-/-}$ mAsts overexpressing individual PDGFRα mutants. Corresponding total proteins or β-actin were used as loading controls. Vertical lines in left panels of p-Tyr, PDGFRα, and β-actin indicate that these images were modified by removal of two lanes of samples between WT and R627. The longer white vertical line indicates that the samples were analyzed in separate SDS-PAGE gels due to the limit of sample loading per gel. (**C** and **D**) Soft agar assay. (**C**) Representative images of soft agar colonies. (**D**) Quantification of soft agar assays. Data are presented as mean ± SD and are representative of 2 independent experiments. Scale bars: 1 mm. $^{*}P < 0.01$.

p-Erk1/2 in mAsts (Supplemental Figure 4C), also inhibited soft agar growth of these cells (Figure 5A), validating Erk1/2 as a mediator of PDGFRα–SHP-2 signaling. Taken together, these data demonstrate that the PDGFRα/PDGF-A–enhanced tumorigenicity of *Ink4a/Arf*-deficient mAsts and human glioma cells requires intact SHP-2 and PI3K enzymatic activities.

*SHP-2 ablation disrupts PI3K/AKT/mTORC1/S6K activation and attenuates the enhanced tumorigenesis of PDGFRα-expressing mAsts.* We then examined the impact of SHP-2 inhibitors (PHPS-1 and NSC87877) and PDGFRα-F720 on PI3K signaling. As shown in Figure 5B and Figure 8A, PDGFRα-F720 mutant and SHP-2 inhibitors significantly decreased PDGF-A–stimulated p-Akt in PDGFRα-expressing mAsts. A nearly complete knockdown of SHP-2 by siRNAs markedly reduced the stimulated p-Akt levels in these cells, possibly through interruption of the association between PI3K (p85 subunit) and PDGFRα (Figure 8B). However, a previous study showed that PDGFRα-F720 mutation did not result in a decrease in PI3K association with the RTK in mouse fibroblasts (10). Similarly, when SHP-2 was knocked down in NIH3T3 cells, a minimal impact of SHP-2 inhibition on PDGF-A–induced PI3K association and Akt phosphorylation was observed in these fibroblasts (Supplemental Figure 5A), suggesting that the impact of SHP-2 on PI3K association with the RTK and p-Akt in astrocytes and glioma cells was specific. To examine whether the effect of SHP-2 knockdown on p-Akt signaling was specific to PDGFRα signaling, we knocked down SHP-2 by siRNAs in EGFRvIII-expressing *Ink4a/Arf*$^{-/-}$ mAsts (WT PTEN) and LN444 and U87MG (both PTEN mutant) cells. We observed a reduction or a modest impact of p-AKT level in LN444/EGFRvIII and U87MG/EGFRvIII cells, respectively (Supplemental Figure 5B), suggesting that SHP-2 also regulates PI3K/AKT activation in other RTK signaling. However, Akt phosphorylation was absent in *Ink4a/Arf*$^{-/-}$ EGFRvIII mAsts, possibly due to the presence of WT Pten in these cells.

We next tested whether signaling downstream to Akt was affected by SHP-2 inhibition. We found that SHP-2 inhibitors (Figure 8A), SHP-2 siRNA knockdown (Figure 8B), or PDGFRα-F731/42 and PDGFRα-F720 mutations (Figure 8C) significantly impaired PDGF-A–stimulated phosphorylation of S6 kinase (p-S6K) downstream to the mammalian target of rapamycin (mTOR) pathway. Thus we further determined the impact of the ablation of SHP-2 and its downstream target the mTOR pathway on cell transformation. Strikingly, stable knockdown of SHP-2 by shRNAs markedly reduced PDGFRα-promoted soft agar growth of mAsts (Figure 8D). Additionally, treatment with mTOR complex 1 (mTORC1) inhibitor rapamycin led to a dose-dependent decrease in soft agar colonies formed by PDGF-A–stimulated *Ink4a/Arf*$^{-/-}$ mAsts expressing PDGFRα or LN444 cells (Supplemental Figure 6, A and B), compared with their respective DMSO-treated controls.

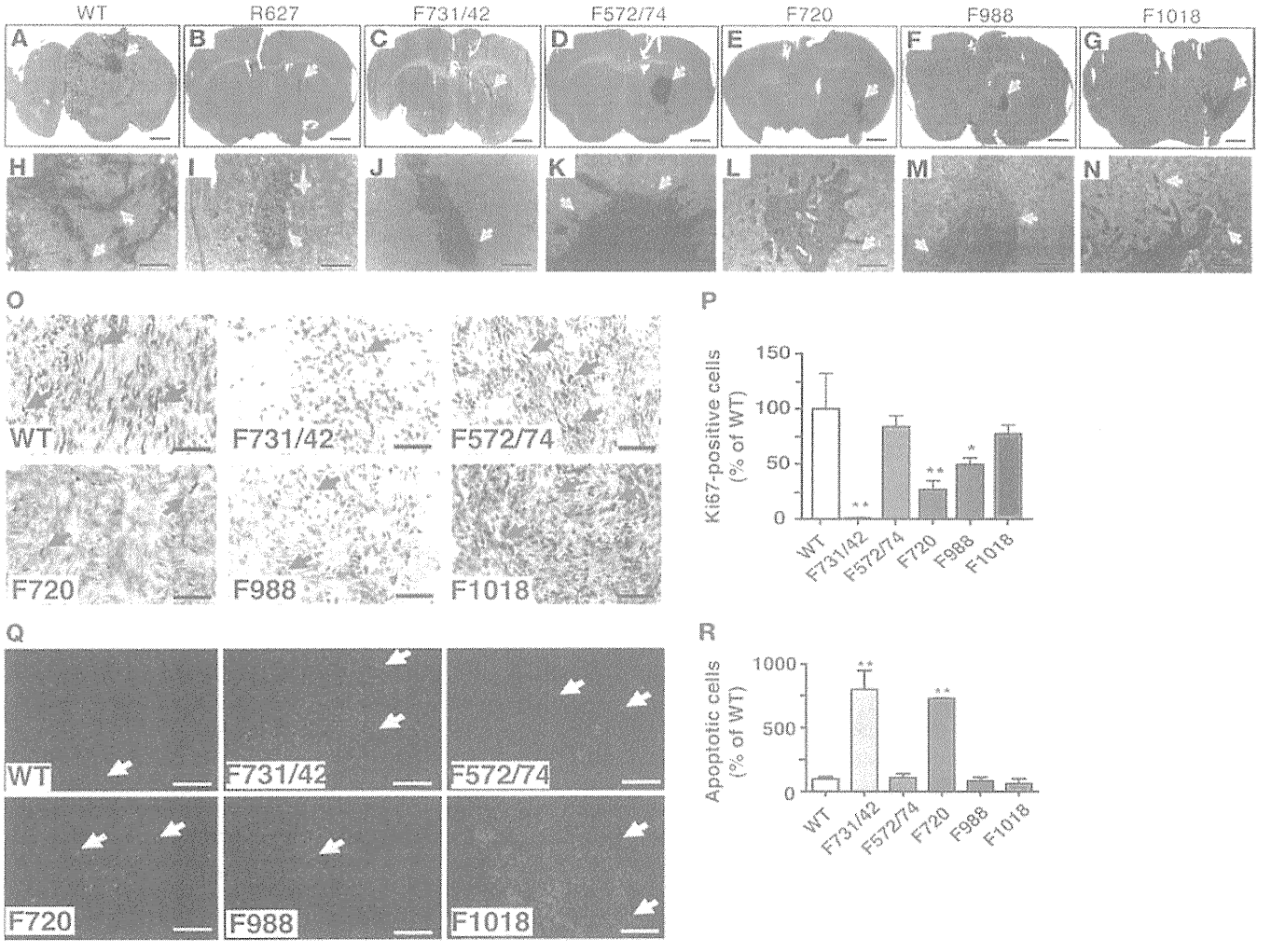


**Figure 6**

Impacts of individual mutations of PDGFRα in mAsts on brain tumorigenesis. (**A**–**N**) Representative H&E staining images of various brain sections from 2 independent experiments with at least 5 mice per group with similar results. Mice that received various types of cells displayed similar tumor onset and survival times as described in Figure 1. Brains were harvested 25–30 days (**A**), 30–35 days (**B**, **C**, **D**, and **G**), and 35–40 days (**E** and **F**) after transplantation. Scale bars: 1 mm (**A**–**G**), 200 μm (**H**–**N**). Arrows indicate tumors or invading cells. (**O**) Ki-67 staining of brain sections. Scale bars: 50 μm. Arrows indicate Ki-67–positive cells. (**P**) Quantification of Ki-67 staining. (**Q**) TUNEL staining images. Scale bars: 100 μm. (**R**) Quantification of TUNEL staining. Data in **P** and **R** are presented as mean ± SD. $^{*}P < 0.01$; $^{**}P < 0.001$.

Similarly, rapamycin was able to effectively suppress the cell transformation capacity conferred by EGFRvIII expression in these cells (Supplemental Figure 6C). Previous studies suggested that the limited efficacy of rapamycin in clinical use was due to the capacity of rapamycin to potentiate PI3K/Akt signaling (24). However, we did not observe an increase of p-Akt level in both *Ink4a/Arf*-deficient mAsts and LN444 cells treated with rapamycin up to 72 hours (Supplemental Figure 6D). These results suggest that PDGFRα-promoted tumorigenesis necessitates an intact SHP-2 activity that regulates the PI3K/AKT/mTOR pathway. Since, in clinical glioblastomas, constitutively active PI3K mutations are mostly observed in specimens with no *PDGFRA* aberrations (3, 4), we introduced a constitutively active PI3K p110 subunit (p110α-CAAX) into *Ink4a/Arf*$^{-/-}$ mAsts that either expressed PDGFRα-F720 or an SHP-2 shRNA. In both cell lines, we observed a rescue effect of p110α-CAAX in soft agar colony formation (Figure 8E), suggesting that PI3K/AKT/mTOR acts downstream of SHP-2 in PDGFRα-overexpressing gliomas, and that activating PI3K mutations in clinical gliomas might be able to bypass SHP-2 activation to promote tumorigenesis. Taken together, our results suggest that SHP-2 regulates the PI3K/AKT/mTOR signaling emanating from PDGFRα activation.

*PDGFRα and PDGF-A are co-expressed, and their expression is linked with the activation of the SHP-2 and the PI3K/AKT/mTOR signaling in clinical glioblastomas.* To determine whether PDGF-A and PDGFRα are co-expressed and whether there is a link of overexpression of PDGF-A and PDGFRα and activation of the SHP-2 and the PI3K/AKT/mTOR signaling in clinical glioma specimens, we performed IHC staining on a total of 158 paraffin-embedded primary human glioma specimens using anti-PDGFRα, anti–PDGF-A, anti–p-SHP-2 Tyr542, anti–p-AKT Ser473, and anti–p-S6 Ser235/236 antibodies. PDGFRα proteins were detected at medium to high levels in 17 of 87 GBMs (WHO grade IV tumors) and in 9 of 71 grade II and III tumors. Among these PDGFRα-positive gliomas,

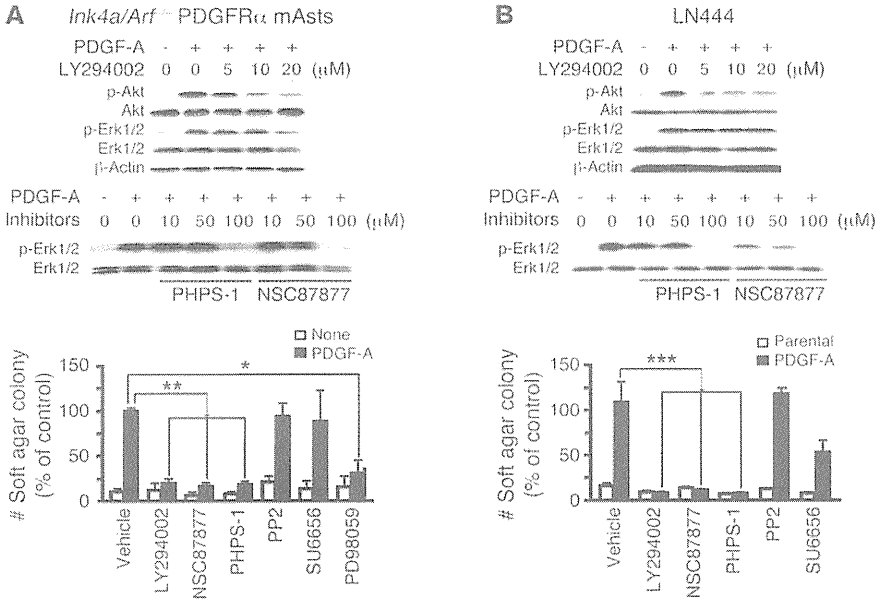


**Figure 7**

Inhibition of PI3K or SHP-2 activities suppresses PDGFRα-stimulated signaling and cell transformation. (**A**) Inhibitors of PI3K (LY294002), SHP-2 (PHPS-1 and NSC87877), and MEK (PD98059), but not SFK (SU6656 and PP2), abrogate cell transformation of PDGFRα-overexpressing *Ink4a/Arf*$^{-/-}$ mAsts. Top and middle: IB analyses. Bottom: Quantification of soft agar assays. Cells were grown in triplicate in soft agar with or without LY294002 (10 μM), PHPS-1 (100 μM), NSC87877 (100 μM), PP2 (5 μM), SU6656 (5 μM), or PD98059 (10 μM). (**B**) PI3K and SHP-2 inhibitors suppress PDGF-A–promoted soft agar growth of *INK4A/ARF*-deficient LN444 glioma cells. Top and middle: IB analysis. Bottom: Soft agar assays. Concentrations of the inhibitors and experimental conditions were identical to those in **A**. Data are presented as mean ± SD. For IB analyses, corresponding total proteins or β-actin were used as loading controls. All data are representative of 2 independent experiments. $^{*}P < 0.001$; $^{**}P < 0.0001$; $^{***}P < 0.01$.

PDGF-A was often co-expressed in the same population of tumor cells (Figure 9, B and C, and Supplemental Table 1). Significantly, phosphorylation of SHP-2 Y542 (p-SHP-2, required for activation of SHP-2) (25), AKT (p-AKT), and ribosomal S6 subunit (p-S6) was also often detected on sister sections of the same tumor in many of the PDGF-A/PDGFRα–positive glioma specimens (Figure 9, B–F, and Supplemental Table 1), suggesting a link between activation of PDGF-A/PDGFRα and stimulation of SHP-2, AKT, and mTOR in clinical glioblastoma specimens. To validate these data, we performed IB analyses on a separate cohort of a total of 20 snap-frozen clinical GBM specimens. As shown in Figure 9G, PDGFRα was expressed at high levels in 7 of 20 GBM samples, 5 of which expressed PDGF-A proteins, suggesting an autocrine PDGFRα signaling in these tumors. In 4 of these 5 PDGF-A/PDGFRα–positive tumors, p-AKT, p-SHP-2, and p-S6 were also detected. Of note, expression of PDGF-A, p-AKT, p-SHP-2, and p-S6 at various levels in other tumor samples likely reflects the impact of heterogeneous gene alterations such as mutations of PTEN, TP53, and overexpression of EGFR/EGFRvIII and c-MET that affect the expression or activation (phosphorylation) of these proteins in clinical glioblastomas. Taken together, these results establish a link of PDGF-A/PDGFRα expression with activation of SHP-2 and PI3K/AKT/mTOR signaling in clinical glioblastoma samples.

## Discussion

In this study, we report that PDGFRα and/or PDGF-A overexpression is able to drive gliomagenesis of *Ink4a/Arf*-deficient mAsts and human glioma LN444 and LN443 cells. Re-introduction of p16INK4a but not p19ARF into *Ink4a/Arf*-null mAsts suppresses PDGFRα-promoted tumor growth. In the absence of PI3K or SHP-2 signaling, PDGFRα fails to enhance tumorigenesis in the brain of mice. Additionally, we establish a link between activation of SHP-2 and the PI3K/AKT/mTOR signaling in PDGFRα-stimulated tumorigenesis in vitro, in mice, and in clinical glioblastoma specimens. Therefore, our data demonstrate that co-alteration of the RTK PDGFRα and tumor suppressor p16INK4a is required for gliomagenesis and that SHP-2 is a critical linker between the PI3K/AKT/mTOR pathway and PDGFRα in the formation of gliomas.

A unique feature of this study is that specific activation of PDGFRα signaling in vivo by PDGF-A, a ligand that binds to PDGFRα but not PDGFRβ (14) as an autocrine loop significantly enhanced the tumorigenesis of *Ink4a/Arf*-deficient mAsts and human glioma cells in the brain. Early studies of clinical glioma specimens showed that PDGF-A and PDGFRα are overexpressed in tumor cells, while PDGF-B and PDGFRβ are expressed in hyperplastic capillaries, suggesting both autocrine and paracrine loops for PDGF/PDGFR activation in gliomas (15). In neonate and adult mice, expression of PDGF-B induces de novo gliomas from GFAP-positive astrocytes and nestin-expressing glial progenitor cells through activation of PDGFRα and PDGFRβ in the brain of both WT and *Ink4a/Arf*-deficient animals (26, 27). Moreover, in WT *Ink4a/Arf* mice, infusion of PDGF-A proteins into the lateral ventricle stimulated tumor-like growth of PDGFRα-positive NSCs in the SVZ in the brain (17). Importantly, data from The Cancer Genome Atlas (TCGA) and other studies revealed that PDGFRα is overexpressed and amplified and often co-expressed with PDGF-A in clinical glioblastoma samples (3, 28, 29). Our results not only functionally validated these studies but also further demonstrated the significance of specific activation of PDGFRα signaling by PDGF-A in cooperation with loss of p16INK4a but not p19ARF in promoting gliomagenesis. We found that when PDGFRα signaling is activated in *Ink4a/Arf*$^{-/-}$ mAsts or human glioma cells, mice that received these cells developed significantly larger and highly invasive tumors in the brain. In contrast, no enhancement of tumorigenesis was found in mice that received glioma cells with PDGFRα and an intact *CDKN2A* locus (19). Together, our studies indicate that PDGFRα activation together with *Ink4a/Arf* loss results in enhanced tumor growth of both mAsts and human glioma cells in the brain.

Tumor suppressor P16INK4A is frequently mutated in clinical glioblastomas (3, 4, 29). In mice, loss of p16INK4a and p19ARF was shown to be indispensable in facilitating tumorigenesis (6). *Ink4a/Arf*-deficient mice were viable and developed spontaneous

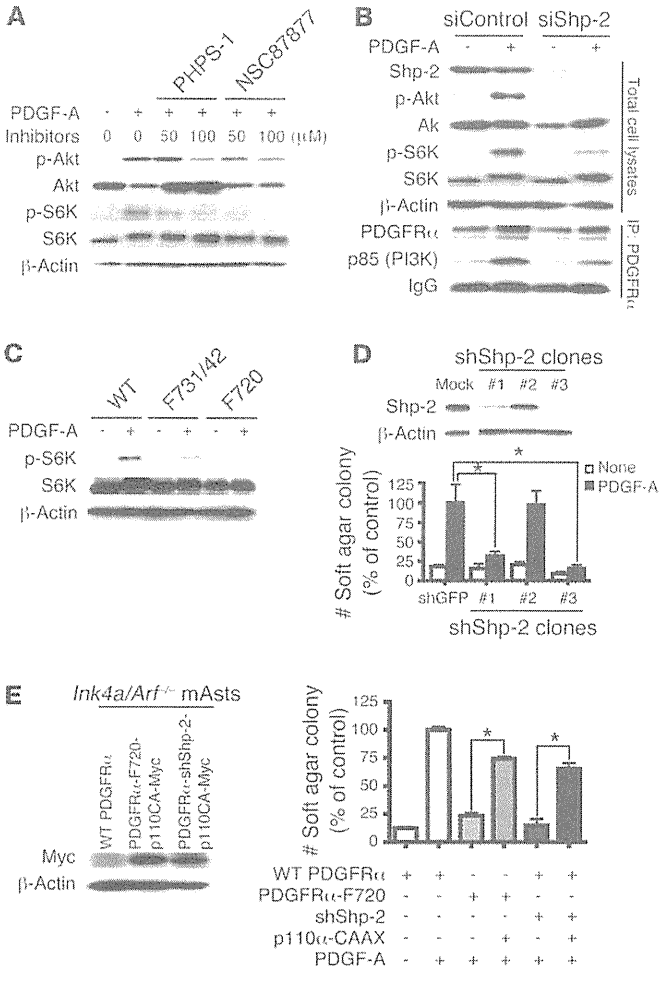


**Figure 8**

SHP-2 recruits PI3K to activate AKT/mTOR/S6K pathway in PDGFRα/PDGF-A–mediated tumorigenesis. (**A**) IB analyses of serum-starved *Ink4a/Arf*$^{-/-}$ PDGFRα-expressing mAsts treated with SHP-2 inhibitors PHPS-1 or NSC87877 for 24 hours followed by 50 ng/ml PDGF-A for 5 minutes. (**B**) IP/IB analysis of PDGFRα-overexpressing mAsts that were transfected with SHP-2 siRNA for 48 hours and serum starved for an additional 24 hours, followed by PDGF-A stimulation. (**C**) IB analysis of phospho-S6 kinase levels of various mAsts stimulated by PDGF-A. (**D**) SHP-2 shRNAs suppressed soft agar growth of mAsts. Top: IB analysis. Bottom: Clones that had a significant decrease in SHP-2 expression (#1 and #3 in top panel) showed reduced tumor cell growth in soft agar. Data are presented as mean ± SD. $^*P < 0.01$, Student's *t* test. (**E**) Constitutively activated PI3K rescued the inhibitory effect of SHP-2 inhibition on blocking PDGFRα-mediated cell transformation. Left: IB analysis of expression of p110α-CAAX. Right: Soft agar assays. Data are presented as mean ± SEM. $^*P < 0.0001$. For all IB analyses, corresponding total proteins, β-actin, or total pulled-down IgG were used as loading controls. All data are representative of 2 to 3 independent experiments.

tumors at early ages, but without detectable tumors in the brain (6, 7). Further studies showed that *Ink4a/Arf* loss cooperates with oncogenic K-Ras, EGFRvIII, or PDGF-B expression in promoting gliomagenesis in the brain (7, 8, 16, 26, 27). However, compared with p16INK4a loss, which contributes to tumor initiation from mAsts, p19ARF deficiency was shown to display a more pronounced impact on cell transformation and gliomagenesis (30, 31). Our data corroborate and also differ from these studies. We showed that re-expression of p16INK4a but not p19ARF in PDGFRα-expressing *Ink4a/Arf*$^{-/-}$ mAsts inhibited tumorigenesis. Inhibition of CDK4/6, the direct target of p16INKa by a specific inhibitor (20), in *Ink4a/Arf*$^{-/-}$ mAsts and glioma cells attenuated PDGF-A stimulation of soft agar growth, suggesting that CDK4/6/p-RB signaling is required for PDGFRα-induced tumorigenesis. On the contrary, although p53 was functional in *Ink4a/Arf*$^{-/-}$ PDGFRα-expressing mAsts, p19ARF was unable to suppress soft agar growth of these cells. Since p19ARF derepresses p53 signaling while PI3K/Akt activates p53 E3 ubiquitin ligase Mdm2 (32), it is plausible that the robust PI3K/Akt activation in PDGFRα-overexpressing cells triggers Mdm2-mediated p53 degradation and thereby renders tumorigenic mAsts resistant to p19ARF inhibition (21). It is also likely that loss of p19ARF is required for survival of glioma cells under certain situations, such as treatment of DNA damage–inducing agent CDDP (Supplemental Figure 3). At least during the initiation or maintenance of cell transformation, p19ARF loss appears to be dispensable (30, 31), since knockdown of *INK4A* alone in WT *INK4A/ARF* LN319 glioma cells restored PDGFRα stimulation of anchorage-independent growth in soft agar. Taken together, these data suggest that loss of p16INK4a plays a predominant role in PDGFRα-promoted gliomagenesis.

The third important aspect in this study is that we functionally assigned signal modules of PDGFRα in promoting gliomagenesis and tumor invasion in the brain of mice. Previous studies by uncoupling individual signaling pathways from PDGFRα using a series of F-to-Y mutants revealed unequal contributions of each signaling pathway emanating from PDGFRα activation (11, 12, 14). Our in vivo and biochemical data corroborate these reports. When compared with WT PDGFRα overexpression, loss of intrinsic tyrosine kinase activity (R627) of the RTK or binding capacity to PI3K (F731/42) or SHP-2 (F720) abrogated PDGFRα-promoted gliomagenesis, thus signifying the central roles of PI3K and SHP-2 signaling in PDGFRα function. However, while disruption of PDGFRα association with SFKs (F572/74) or PLCγ (F1018) only had a moderate impact on tumor formation in the brain, significant inhibition of tumor cell infiltration in the brain was seen in these tumors, as compared with the WT PDGFRα tumors, thus validating the role of SFKs and PLCγ in mediating PDGFRα-stimulated cell invasion (10). Moreover, a separate set of experiments with individual "add-back panel" mutants in

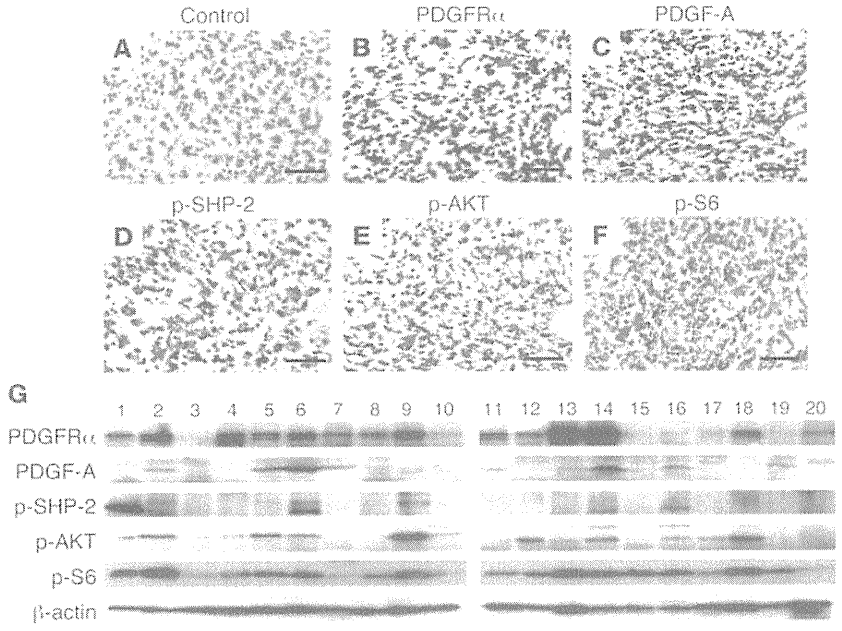


**Figure 9**
PDGFRα and PDGF-A are co-expressed in clinical glioma specimens with activated SHP-2 and PI3K/AKT/mTOR pathways. (**A**–**F**) Images of IHC staining on sister sections of a representative human J212 GBM specimen, using anti-PDGFRα (**B**), anti–PDGF-A (**C**), anti–p–SHP-2 (Y542) (**D**), anti–p-AKT (**E**), and anti–p-S6 (**F**) antibodies. (**A**) No primary antibody. Arrows indicate positive staining for the indicated proteins. Scale bars: 50 μm. (**G**) IB analysis of tissue lysates of a separate cohort of 20 human GBM snap-frozen specimens using indicated antibodies. β-Actin was used as a loading control. Data are representative of 2 independent experiments with similar results.

which 1 of 5 signal modules was individually retained as single or double Y residues (Y731/42, Y572/74, Y720, Y988, and Y1018) could not fully restore PDGFRα-promoted tumorigenesis in the brain (data not shown), consistent with the previous findings using an identical set of PDGFRα add-back panel mutants (10). It is plausible that, similar to this previous in vitro study (10), in which retention of a combination of 2 or 3 add-back signaling modules with comparable levels of total RTK protein in WT PDGFRα–expressing cells was able to restore PDGFRα-mediated biological responses, co-activation of PI3K (Y731/42)– and SHP-2 (Y720)–mediated signaling may be required for the full spectrum of WT PDGFRα–promoted gliomagenesis in the brain.

The last (and what we believe is also the most novel) finding in this study is the emergence of SHP-2 as an essential mediator in PDGFRα-promoted gliomagenesis. SHP-2 (encoded by *PTPN11* gene) is a protein tyrosine phosphatase (PTP) identified as a bona fide proto-oncogene that activates Ras/MAPK signaling through a yet-to-be-defined mechanism (33). Additionally, the role of SHP-2 in mediating PDGFRα signaling has not been clear (9, 11, 14). In human cancers including GBMs, mutations of SHP-2 or its binding partners have been reported, leading to sustained Ras/MAPK signaling (34, 35). Recent genomic analysis of TCGA data has designated *PTPN11* as one of the 6 "linker" genes, which are statistically enriched for connections to various GBM altered genes, thus suggesting a critical role for SHP-2/*PTPN11* in modulation of downstream biological signaling in gliomagenesis (36). Our data not only establish the critical role of SHP-2 in mediating PDGFRα activation for glioma formation but also functionally validate this hypothesis. We showed that inhibition of SHP-2 function by removal of its binding module in PDGFRα (F720 mutant), gene knockdown or pharmacological inhibitors significantly impaired PDGFRα stimulation of tumorigenesis in vivo and in vitro and its downstream signaling effectors, Erk1/2 and PI3K/Akt/mTOR in *Ink4a/Arf*-deficient mAsts and glioma cells. Significantly, re-expression of a constitutively active p110, the catalytic subunit of PI3K, rescued the inhibition of SHP-2 in *Ink4a/Arf*-deficient mAsts. In EGFRvIII-expressing U87MG glioma cells, SHP-2 regulates activities of ERK/2 and CDC2 that modulate cell cycle progression but has a minimal effect on AKT activation (23). On the contrary, we found that knockdown of SHP-2 not only attenuated PDGFRα stimulation of Erk1/2 activity but also impaired PI3K/Akt/mTOR activity in *Ink4a/Arf*-deficient mAsts and human glioma cells. The impact of inhibition of SHP-2 on PI3K/Akt signaling appears to be specific in astrocytic tumors, since we did not observe inhibited PDGF-A stimulation of p-Akt or association of PI3K with PDGFRα in SHP-2–knockdown NIH3T3 fibroblasts. On the other hand, the MEK inhibitor PD98059 also reduced the tumorigenicity of *Ink4a/Arf*-deficient mAsts, indicating that SHP-2–mediated PDGFRα signaling requires not only PI3K/Akt but also Erk1/2 activation in gliomagenesis. Additionally, SHP-2 was found to either positively or negatively regulate PI3K/AKT activity (34). However, in our model systems, SHP-2 is required for full activation of PI3K/Akt/mTOR, and inhibition of mTOR by rapamycin markedly suppressed PDGFRα-promoted tumorigenesis. These data are significant since a recent proteomic study revealed that mTOR signaling is predominantly activated in "*PDGFRA* co-cluster" glioblastomas (37), thus corroborating our observations. However, since phosphorylation of Akt Ser473 occurs both upstream and downstream of mTORC2 signaling, our data do not rule out the role of mTORC2 in PDGFRα-activated signaling. Lastly, our data also demonstrated the importance of activation of PI3K/mTOR signaling by SHP-2 in PDGFRα- or EGFRvIII-promoted tumorigenesis. Taken together, our findings suggest SHP-2 as a critical modulator that regulates PDGFRα-mediated PI3K/AKT/mTOR activities in the development of malignant glioblastomas.

In summary, this study provides molecular insights into the mechanisms by which *PDGFRA* amplification together with loss of *INK4A/ARF* promotes gliomagenesis in the brain. Our data identified SHP-2, as well as PI3K, as a pivotal mediator of PDGFRα signaling in glioma formation. These results have direct clinical relevance, since we not only establish a model system to demonstrate the co-operative role of *PDGFRA* overexpression and *INK4A/ARF* loss in clinical glioblastomas, but also provide functional evidence to validate genomic analyses demonstrating that SHP-2/*PTPN11* is an essential "linker" among glioma altered genes (36). Secondly, activated mTOR

signaling is predominantly found within the subclass of glioblastomas with abnormal PDGFRα signaling (37). Finally, constitutively active PI3K mutations (*PIK3CA* and *PIK3R1*) occur mostly in clinical glioblastomas without *PDGFRA* aberrations (4). Consequently, our results strongly suggest SHP-2/*PTPN11* as a potential target for treatments of glioblastomas with *PDGFRA* overexpression.

## Methods

*Cell lines and reagents.* Primary *Ink4a/Arf*$^{-/-}$ mAsts were derived and propagated as previously described (7). Human glioma cell lines LN444, LN443, LN-Z308, and LN319 were obtained from ATCC or from our own collection (38). Unless otherwise mentioned, all glioma cell lines and primary mAsts were routinely maintained in 5% $CO_2$ at 37°C, in DMEM (Invitrogen) containing 10% FBS (Hyclone), 100 U/ml penicillin, and 100 μg/ml streptomycin (Invitrogen).

*Histology and IHC.* Studies using human tissues were reviewed and approved by the Institutional Review Board involving Human Subjects of the University of Pittsburgh. The specimens were de-identified human tissues, and thus no informed consent was required. A total of 158 paraffin-embedded thin sections of primary human glioma specimens were used, including 87 WHO grade IV GBMs, 34 grade III anaplastic astrocytomas, anaplastic oligodendrogliomas, or anaplastic oligodendroastrocytomas, and 37 grade II oligodendrogliomas and diffuse astrocytomas. Thin sections of human glioma specimens and mouse brains with various tumors were analyzed by IHC using indicated (e.g., Figure 8 legend and Results) antibodies or a TUNEL staining kit as previously described (38, 39). Briefly, the 5-μm human tissue sections were deparaffinized in xylene, followed by rehydration in graded ethanol. After washing with TBS, the antigen was retrieved by boiling the sections in a citrate buffer (pH 6.0) twice for 5 minutes. For mouse brain tissues with various gliomas, 5-μm frozen sections were fixed in pre-chilled acetone at –20°C for 5 minutes, rinsed with PBS, and blocked by AquaBlock (East Coast Biologics Inc.) for 1 hour at room temperature. Afterward, various tissue sections were then incubated with a primary antibody overnight at 4°C and blocked by Peroxidase Blocking Reagent (DAKO) for 10 minutes, followed by incubation with a biotinylated secondary antibody for 30 minutes at room temperature. After washing in PBS, stained tissue sections were visualized by diaminobenzidine chromophore and $H_2O_2$, followed by hematoxylin counterstaining. Sections were then dehydrated by graded ethanol and mounted with Permount Solution (Fisher).

*Soft agar colony formation assay.* Colony formation assay in soft agar was performed as previously described (40). Briefly, approximately 5,000 cells were seeded in a 0.5% Noble Agar top layer with a bottom layer of 0.8% Noble Agar in each of the triplicate wells of a 24-well plate. Growth factor–reduced Matrigel (1 mg/ml) was added into the top layer with or without inhibitors as indicated in figure legends (e.g., Figure 7 legend) and described in Results. PDGF-A–expressing cells in 10% of total cells were included as a source of PDGF-A. DMEM containing 10% FBS was added 3 days after plating and changed every 3 days thereafter. Colonies were scored after 2–3 weeks using Olympus SZX12 stereomicroscope, and data were analyzed using GraphPad Software.

*Mouse glioma xenografts, IP, IB, tissue image analyses and quantifications, and siRNA.* Experiments of mouse glioma xenografts, IP, IB, tissue imaging and analyses, and siRNA knockdown were performed as previously described (39). For details, see Supplemental Experimental Procedures.

*Statistics.* One-way ANOVA or an unpaired, 2-tailed Student's *t* test followed by Newman-Keuls post-test was performed using GraphPad Prism software. A *P* value of 0.05 or less was considered statistically significant.

## Acknowledgments

We would like to thank Carl-Henrik Heldin at Uppsala University for PDGFRα and PDGF-A cDNAs, Russell O. Pieper at University of California San Francisco for pMXI-*gfp* retroviral vector, Lynda Chin at Dana-Farber Cancer Institute for the cDNA of p16INK4a, Yi Zheng at Cincinnati Children's Hospital Medical Center for cDNA of p19ARF, Tao Cheng at University of Pittsburgh for pMSCV retroviral vectors, and N. Balass for proofreading the manuscript. This work was supported by grants from the NIH (CA102011 and CA130966 to S.-Y. Cheng; EY012509 to A. Kazlauskas; CA87375 to K. Symes), American Cancer Society (RSG CSM-107144), and Pennsylvania Department of Health and Innovative Research Scholar Awards of the Hillman Foundation (to S.-Y. Cheng and B. Hu).

Received for publication May 13, 2010, and accepted in revised form December 22, 2010.

Address correspondence to: Bo Hu, University of Pittsburgh Cancer Institute and Department of Medicine, 5117 Centre Avenue, 2.26, Pittsburgh, Pennsylvania 15213, USA. Phone: 412.623.7791; Fax: 412.623.4840; E-mail: hub@upmc.edu. Or to: Shi-Yuan Cheng, University of Pittsburgh Cancer Institute and Department of Pathology, 5117 Centre Avenue, 2.26f, Pittsburgh, Pennsylvania 15213, USA. Phone: 412.623.3261; Fax: 412.623.4840; E-mail: chengs@upmc.edu.

1. Wen PY, Kesari S. Malignant gliomas in adults. *N Engl J Med.* 2008;359(5):492–507.
2. Furnari FB, et al. Malignant astrocytic glioma: genetics, biology, and paths to treatment. *Genes Dev.* 2007;21(21):2683–2710.
3. TCGA. Comprehensive genomic characterization defines human glioblastoma genes and core pathways. *Nature.* 2008;455(7216):1061–1068.
4. Verhaak RG, et al. Integrated genomic analysis identifies clinically relevant subtypes of glioblastoma characterized by abnormalities in PDGFRA, IDH1, EGFR, and NF1. *Cancer Cell.* 2010;17(1):98–110.
5. Sherr CJ. The INK4a/ARF network in tumour suppression. *Nat Rev Mol Cell Biol.* 2001;2(10):731–737.
6. Serrano M, Lee H, Chin L, Cordon-Cardo C, Beach D, DePinho RA. Role of the INK4a locus in tumor suppression and cell mortality. *Cell.* 1996;85(1):27–37.
7. Bachoo RM, et al. Epidermal growth factor receptor and Ink4a/Arf: convergent mechanisms governing terminal differentiation and transformation along the neural stem cell to astrocyte axis. *Cancer Cell.* 2002;1(3):269–277.
8. Uhrbom L, Dai C, Celestino JC, Rosenblum MK, Fuller GN, Holland EC. Ink4a-Arf loss cooperates with KRas activation in astrocytes and neural progenitors to generate glioblastomas of various morphologies depending on activated Akt. *Cancer Res.* 2002;62(19):5551–5558.
9. Heldin CH, Ostman A, Ronnstrand L. Signal transduction via platelet-derived growth factor receptors. *Biochim Biophys Acta.* 1998;1378(1):F79–F113.
10. Rosenkranz S, DeMali KA, Gelderloos JA, Bazenet C, Kazlauskas A. Identification of the receptor-associated signaling enzymes that are required for platelet-derived growth factor-AA-dependent chemotaxis and DNA synthesis. *J Biol Chem.* 1999; 274(40):28335–28343.
11. Bertsholtz C. Insight into the physiological functions of PDGF through genetic studies in mice. *Cytokine Growth Factor Rev.* 2004;15(4):215–228.
12. Van Stry M, Kazlauskas A, Schreiber SL, Symes K. Distinct effectors of platelet-derived growth factor receptor-alpha signaling are required for cell survival during embryogenesis. *Proc Natl Acad Sci U S A.* 2005;102(23):8233–8238.
13. Klinghoffer RA, Hamilton TG, Hoch R, Soriano P. An allelic series at the PDGFalphaR locus indicates unequal contributions of distinct signaling pathways during development. *Dev Cell.* 2002;2(1):103–113.
14. Tallquist M, Kazlauskas A. PDGF signaling in cells and mice. *Cytokine Growth Factor Rev.* 2004;15(4):205–213.
15. Hermanson M, et al. Platelet-derived growth factor and its receptors in human glioma tissue: expression of messenger RNA and protein suggests the presence of autocrine and paracrine loops. *Cancer Res.* 1992;52(11):3213–3219.
16. Dai C, Celestino JC, Okada Y, Louis DN, Fuller GN, Holland EC. PDGF autocrine stimulation dedifferentiates cultured astrocytes and induces oligodendrogliomas and oligoastrocytomas from neural progenitors and astrocytes in vivo. *Genes Dev.* 2001;15(15):1913–1925.
17. Jackson EL, et al. PDGFR alpha-positive B cells are neural stem cells in the adult SVZ that form glioma-like growths in response to increased PDGF signaling. *Neuron.* 2006;51(2):187–199.
18. Stallcup WB, Huang FJ. A role for the NG2 proteoglycan in glioma progression. *Cell Adh Migr.* 2008;2(3):192–201.
19. Ishii N, et al. Frequent co-alterations of TP53, p16/CDKN2A, p14ARF, PTEN tumor suppres-

sor genes in human glioma cell lines. *Brain Pathol.* 1999;9(3):469–479.
20. Wiedemeyer WR, et al. Pattern of retinoblastoma pathway inactivation dictates response to CDK4/6 inhibition in GBM. *Proc Natl Acad Sci U S A.* 2010; 107(25):11501–11506.
21. Fraser M, Bai T, Tsang BK. Akt promotes cisplatin resistance in human ovarian cancer cells through inhibition of p53 phosphorylation and nuclear function. *Int J Cancer.* 2008;122(3):534–546.
22. Wu CJ, O'Rourke DM, Feng GS, Johnson GR, Wang Q, Greene MI. The tyrosine phosphatase SHP-2 is required for mediating phosphatidylinositol 3-kinase/Akt activation by growth factors. *Oncogene.* 2001;20(42):6018–6025.
23. Zhan Y, Counelis GJ, O'Rourke DM. The protein tyrosine phosphatase SHP-2 is required for EGFRvIII oncogenic transformation in human glioblastoma cells. *Exp Cell Res.* 2009;315(14):2343–2357.
24. Wan X, Harkavy B, Shen N, Grohar P, Helman LJ. Rapamycin induces feedback activation of Akt signaling through an IGF-1R-dependent mechanism. *Oncogene.* 2007;26(13):1932–1940.
25. Lu W, Gong D, Bar-Sagi D, Cole PA. Site-specific incorporation of a phosphotyrosine mimetic reveals a role for tyrosine phosphorylation of SHP-2 in cell signaling. *Mol Cell.* 2001;8(4):759–769.
26. Hu X, Holland EC. Applications of mouse glioma models in preclinical trials. *Mutat Res.* 2005; 576(1–2):54–65.
27. Calzolari F, Malatesta P. Recent insights into PDGF-Induced gliomagenesis. *Brain Pathol.* 2010;20(3):527–538.
28. Martinho O, et al. Expression, mutation and copy number analysis of platelet-derived growth factor receptor A (PDGFRA) and its ligand PDGFA in gliomas. *Br J Cancer.* 2009;101(6):973–982.
29. Parsons DW, et al. An integrated genomic analysis of human glioblastoma multiforme. *Science.* 2008;321(5897):1807–1812.
30. Sharpless NE, Ramsey MR, Balasubramanian P, Castrillon DH, DePinho RA. The differential impact of p16(INK4a) or p19(ARF) deficiency on cell growth and tumorigenesis. *Oncogene.* 2004;23(2):379–385.
31. Tchougounova E, Kastemar M, Brasater D, Holland EC, Westermark B, Uhrbom L. Loss of Arf causes tumor progression of PDGFB-induced oligodendroglioma. *Oncogene.* 2007;26(43):6289–6296.
32. Mayo LD, Donner DB. The PTEN, Mdm2, p53 tumor suppressor-oncoprotein network. *Trends Biochem Sci.* 2002;27(9):462–467.
33. Matozaki T, Murata Y, Saito Y, Okazawa H, Ohnishi H. Protein tyrosine phosphatase SHP-2: a proto-oncogene product that promotes Ras activation. *Cancer Sci.* 2009;100(10):1786–1793.
34. Chan G, Kalaitzidis D, Neel BG. The tyrosine phosphatase Shp2 (PTPN11) in cancer. *Cancer Metastasis Rev.* 2008;27(2):179–192.
35. Navis AC, van den Eijnden M, Schepens JT, Hooft van Huijsduijnen R, Wesseling P, Hendriks WJ. Protein tyrosine phosphatases in glioma biology. *Acta Neuropathol.* 2010;119(2):157–175.
36. Cerami E, Demir E, Schultz N, Taylor BS, Sander C. Automated network analysis identifies core pathways in glioblastoma. *PLoS One.* 2010;5(2):e8918.
37. Brennan C, et al. Glioblastoma subclasses can be defined by activity among signal transduction pathways and associated genomic alterations. *PLoS One.* 2009;4(11):e7752.
38. Jarzynka MJ, et al. ELMO1 and Dock180, a bipartite Rac1 guanine nucleotide exchange factor, promote human glioma cell invasion. *Cancer Res.* 2007;67(15):7203–7211.
39. Yiin JJ, et al. Slit2 inhibits glioma cell invasion in the brain by suppression of Cdc42 activity. *Neuro Oncol.* 2009;11(6):779–789.
40. Yoshida S, Shimizu E, Ogura T, Takada M, Sone S. Stimulatory effect of reconstituted basement membrane components (matrigel) on the colony formation of a panel of human lung cancer cell lines in soft agar. *J Cancer Res Clin Oncol.* 1997;123(6):301–309.

基本をマスター
# 脳神経外科手術のスタンダード GO→WEB

# 松果体腫瘍の総合的な治療

西川　亮[1) ] 鈴木智成[1)]
Ryo NISHIKAWA, Tomonari SUZUKI
1）埼玉医科大学国際医療センター脳・脊髄腫瘍科　〒350-1298　埼玉県日高市山根1397-1

POINT 1 悪性腫瘍は手術＋放射線療法＋化学療法を組み合わせて治療を行うが，組織型によってそれぞれの重み付けが異なる．

POINT 2 直達手術は，放射線・化学療法後に行うことも考慮する．

POINT 3 胚細胞腫は臨床試験への参加が望ましい．

## はじめに

松果体腫瘍の主たる腫瘍型は胚細胞腫と松果体実質性腫瘍である．それぞれの主要な病理組織学的分類を表1に記した．従来，ジャーミノーマなどの腫瘍は胚細胞腫瘍と呼ばれているが，他の腫瘍型の命名の法則にならって「胚細胞腫」と呼ぶべきであるという指摘がある．胚細胞腫はさらに，その予後の観点から臨床的に3群に分類される（表2）．

成熟奇形腫と松果体細胞腫以外は悪性腫瘍である．悪性腫瘍は手術による摘出だけでは治癒に至らない．手術＋放射線療法＋化学療法を組み合わせることになるが，組織型によってそれぞれの重み付けが異なることを理解しなければならない．

## 神経内視鏡か直達手術か

神経内視鏡による生検を選択するか，直達手術を選択するかという問題には確立した基準はない．神経内視鏡には侵襲が少ないという大きなメリットがあり，また第三脳室開窓術を同時に行うことができるということも有利である．一方，内視鏡生検では小さな検体の採取になるので，組織学的に混合腫瘍の成分を見逃す可能性が否定でき